Accepted Manuscript

Stress evolution and structural inheritance controlling an intracontinental extensional basin: The central-northern sector of the Neogene Teruel Basin

Carlos L. Liesa, José L. Simón, Lope Ezquerro, Luis E. Arlegui, Aránzazu Luzón

PII: S0191-8141(18)30378-X

DOI: https://doi.org/10.1016/j.jsg.2018.11.011

Reference: SG 3778

To appear in: *Journal of Structural Geology*

Received Date: 13 July 2018

Revised Date: 2 November 2018

Accepted Date: 17 November 2018

Stress evolution and structural inheritance controlling an intracontinental extensional basin: the central-northern sector of the Neogene Teruel Basin

Carlos L. Liesa*, José L. Simón, Lope Ezquerro, Luis E. Arlegui, Aránzazu Luzón

Departamento de Ciencias de la Tierra, Facultad de Ciencias, Grupo Geotransfer-Instituto de Investigación en Ciencias Ambientales (IUCA), Universidad de Zaragoza, Pedro Cerbuna 12, 50009 Zaragoza, Spain

- Carlos L. Liesa (carluis@unizar.es) * (Corresponding author)
- José L. Simón: jsimon@unizar.es
- Lope Ezquerro: lope@unizar.es
- Luis E. Arlegui: arlegui@unizar.es
- Aránzazu Luzón: aluzon@unizar.es

Abstract

The Teruel Basin is a NNE-SSW trending intracontinental extensional basin located in central-eastern Iberia. It is asymmetrically bounded to the east by a major fault zone, but intrabasinal faults with diverse orientation (NNE-SSW to NE-SW, E-W, or NW-SE) also appear. Offsets of the successive sedimentary units and of two planation surfaces reveal that tectonic activity initiated at the border faults, while intrabasinal ones mainly developed in a later stage. Fractures on a map scale show a prevailing N-S strike in Neogene synrift rocks, while a dense network made of four main fracture sets (NE-SW, E-W to ESE-WNW, N-S and NNW-SSE), likely inherited from Mesozoic rifting stages, is observed in pre-rift units. The results of palaeostress analyses indicate an overall predominance of σ_3 directions around E-W, although two stress

episodes have been distinguished during the Late Miocene-Pleistocene: (i) triaxial extension with σ_3 E-W; (ii) almost 'radial' extension (σ_1 vertical, $\sigma_2 \approx \sigma_3$) with a somehow prevailing σ_3 ENE-WSW. A scenario in which the evolving extensional stress field was able to gradually activate major basement structures with different orientation, inherited from previous tectonic events, is proposed as responsible for the evolution and overall pattern of both the eastern active margin and central parts of the central-northern sector of the Teruel Basin.

Keywords: fracture; paleostress; stress partitioning; normal fault; extensional basin

1. Introduction

Evolution of active extensional basin margins has been mainly analysed in the light of numerical, analogue or natural models that pay attention to fault interaction and linkage (e.g. Peacock and Sanderson, 1991; Crider and Pollard, 1998; Walsh et al., 1999; Gupta and Scholz, 2000). In most of these models it is assumed that a pre-existing homogeneous rock mass is subjected to a steady-state stress field to produce faults. However, it is more realistic to expect stress fields that change over time and the influence of pre-existing structures in underlying and adjacent rocks.

Development of fracture systems that control extensional basins should be seen in the framework of tectonic stress fields that are heterogeneous both in space and time, due to (i) intrinsic variability of stress sources, (ii) local perturbations, and (iii) rheological contrasts (Caputo, 2005). Changes in tectonic framework could produce changes in the 'local' stress field, hence inducing apparent 'phases' as inferred from distinct fault systems. Deflection of stress trajectories is caused either directly by slip along faults or undirectedly due to mechanical discontinuities (e.g. Rispoli, 1981; Homberg et al., 1997; Simón et al., 1999). Its effect is maximum close to fractures where the resolved shear stress regularly tend to 0 during each seismic cycle and the direction of the maximum horizontal stress (S_{Hmax}) is deflected to become either nearly parallel or nearly orthogonal to the faults (Simón et al., 1988). Relative variations of also the principal stress magnitudes frequently result in permutation or interchange of stress axes (owing to either gradual change in remote stress magnitudes, or release of stress normal to primary fractures subsequent to failure under unvarying remote stress conditions; e.g. Larroque and Laurent, 1988; Bai et al., 2002). Finally, *stress partitioning* represents a further type of stress heterogeneity, conceptually different from both random stress variability, and 'polyphase' tectonics. It appears as systematic, sometimes cyclically sequenced records of distinct stress fields, giving the appearance that the total stress field is decoupled into several components (Simón et al., 2008).

The Neogene Teruel Graben is a noteworthy case of extensional basin developed through varying stress conditions and strongly influenced by structural inheritance. Recent extensional stress fields in the region where initially reconstructed by Simón (1982, 1983, 1989), then refined by Cortés (1999), Liesa (2000, 2011a) and Lafuente (2011). Arlegui et al. (2005, 2006) made an important contribution to that reconstruction by processing abundant fault population data without striation orientations, by using the method proposed by Lisle et al. (2001). The model resulting from such research is a complex regional stress field that evolved through Neogene following three main stages: (i) nearly N-S compression active until Middle Miocene, with σ_1 trajectories frequently flipping between NNW-SSE and NNE-SSW trends; (ii) triaxial extension with σ_3 trajectories oriented W-E to WNW-ESE, prevailing during the Late Miocene; (iii) almost radial extension (σ_1 vertical, $\sigma_2 \approx \sigma_3$) with a generally prevailing σ_3 trending nearly WSW-ENE, mainly since late Pliocene, which commonly undergoes stress deflections, permutations and partitioning.

The evolutionary pattern of faults and fractures (generated during specific tectonic episodes, later reactivated controlling new structural settings) was firstly stablished by Simón (1983, 1989). More detailed analysis of fracture systems, mainly those present in El Pobo Range (east of the Teruel Graben), is due to Liesa (2000, 2011b). The imprint of inherited structures along the tectonic evolution of the region has been revealed by e.g. Liesa et al. (2006) for Mesozoic extensional basins of the Maestrazgo domain, Liesa et al. (2004) or Lafuente et al. (2011) for Palaeogene contractional structures, and Rubio and Simón (2007) for recent extensional faults.

Recently, the PhD study by Ezquerro (2017) has compiled existing information and added new data. The entire data set was analysed with the aim of building an evolutionary model for the Teruel Basin, in which structural, sedimentary, paleoclimatic, geomophological and chronological aspects are fully integrated. The present paper summarizes the main results of that unpublished regional study (Ezquerro, 2017) focusing on stress fields and fracture evolution. In particular, our main goal is to show the role of the inherited pre-rift structures during the basin evolution, and demonstrate how a spatially and temporally heterogeneous stress field selectively reactivated these pre-existing structures.

2. Geological setting

The Neogene, NNE-SSW trending Teruel Basin is located in the central-eastern Iberian Chain (Fig. 1a), cutting obliquely and postdating the Alpine contractional structures (Álvaro et al., 1979). It represents the main onshore structure linked to the Valencia Trough rifting (Simón, 1982), belonging to an extensional fault system detached at a depth of 11-14 km (Roca and Guimerà, 1992). This fault system evolved through two distinct extensional episodes (Simón, 1982, 1983): the first one (Miocene) gave rise to the main NNE-SSW trending grabens (Teruel and Maestrazgo), and the second one (Late Pliocene-Quaternary) originated the NNW-SSE trending Jiloca graben and partly reactivated the Teruel and Maestrazgo structures.

The northern Teruel Basin was filled in endorheic conditions by a continuous sedimentary succession made of alluvial, palustrine, lacustrine and aeolian facies, ranging from Late Miocene

(Vallesian) to Late Pliocene (Villafranchian) in age (e.g. Simón, 1983; Alcalá et al., 2000; Rodríguez-López et al., 2012). These deposits have been divided into four formal lihostratigraphical units (Peral, Alfambra, Tortajada and Escorihuela Formations; Weerd, 1976), as well as into informal units (*Unidad Detrítica Inferior-Rojo 1*, *Calizas Intermedias, Páramo 1*, *Rojo 2*, *Páramo 2*, *Rojo 3* and *Villafranchian Pediment*; Godoy et al., 1983a,b), and genetic units (Alonso-Zarza and Calvo, 2000). More recently, Ezquerro (2017) has defined six genetic units (TN1 to TN6) based on an overall megasequential evolution mainly controlled by tectonics.

The northern sector of the Teruel Basin is a halfgraben bounded by the N-S striking El Pobo Fault Zone (EPFZ) (Fig. 1b). The footwall block (El Pobo Range) consists of Triassic and Jurassic rocks, deformed by interfering NW-SE and NE-SW trending folds and a dense fault grid (Liesa, 2000, 2011a,b; Liesa et al., 2006; Antolín-Tomás et al., 2007). The Neogene infill in the hanging-wall block began during Middle Miocene (Tortonian) times and lay on a widespread planation surface, the *Intramiocene Erosion Surface* (*IES*) (Gutiérrez and Peña, 1976; Peña et al., 1984), which has been recently dated by Ezquero (2017) to ca. 11.2 Ma. The basin infill shows a gentle roll-over monocline expressed as eastwards tilting (1-2°, in average), except for a fringe at the eastern margin where westwards dipping is observed completing a gentle asymmetric syncline. Tilting also affects a planation surface (*Fundamental Erosion Surface*, *FES*, as defined by Peña et al., 1984) correlative of the uppermost, Middle Pliocene lacustrine deposits of the basin, which have permitted dating the *FES* to 3.5 Ma (Ezquerro, 2017). The *IES* and *FES* planation levels represent useful markers for evaluating offsets across the region (e.g. Rubio and Simón, 2007; Simón et al., 2012).

3. Methodology

Structural characterization of the eastern, active margin of the Teruel Graben has been mainly achieved by geological mapping, based on field survey and analysis of aerial images (stereoscopic aerial photographs at 1:18,000 scale; orthorectified satellite imagery at 1:5,000 scale). Also 5 m grid Digital Elevation Models (DEM) have been used for identifying and drawing traces of some faults with morphological expression.

The *IES* and *FES* planantion surfaces, as well as their correlative stratigraphical levels have been used as composite, morpho-sedimentary markers for estimating fault throws since the beginning of Teruel Basin development (Tortonian; 11.2 Ma) to Present. Their altitudes have been recently obtained by Ezquerro (2017) from aerial photographs, field surveys and geological cross-sections. Where such markers are directly observable (e.g., *IES* on top of El Pobo Range and their correlative unconformity at the base of the Neogene succession within the basin) those data have allowed calculating fault throws with a precision of about 10-20 m. Where the position of markers has been reconstructed from cross sections, the uncertainty could increase up to ca. 50 m.

The orthorectified satellite imagery has also allowed detailed mapping of the dense fracture network in Mesozoic units, and to a lesser extent in the Neogene infill. The strike and length of the different traces were automatically processed through vectorial analysis of mapped fractures by using the QGis software. From such data, rose diagrams and frequency histograms (both computing the number of faults and weighted according the fracture length) were constructed.

Palaeostress analyses have been carried out from populations of small-scale faults collected at 24 sites, from which 30 deviatoric stress tensors have been obtained. The protocol for obtaining stress tensors from faults with slickenline orientations include (Casas et al., 1990): (i) a first approach by means of the Right Dihedra method (Angelier and Mechler, 1977) and the y-R diagram (Simón, 1986); (ii) achieving the optimum stress inversion solution(s), including the stress ratio R = $(\sigma_2 - \sigma_3) / (\sigma_1 - \sigma_3)$, using the method proposed by Etchecopar et al. (1981). Analysis of fault samples without slip lineations has been based on the method proposed by Lisle et al. (2001), already successful in this region (Arlegui et al., 2005, 2006), implemented using the computer package FSA of Celérier (2011).

Together with these new palaeostress results, other 61 deviatoric stress tensors inferred at a total of 55 measurement sites all over the northern Teruel Basin have been compiled from previous works, with the purpose of increasing and improving the a palaeostress database to obtain a better picture of the complex Neogene tectonic setting. This task has benefited from an abundant literature (Simón, 1983, 1989; Simón and Paricio, 1988, Cortés, 1999; Arlegui et al., 2005, 2006; Liesa and Simón, 2009; Lafuente, 2011; Liesa, 2011a).

4. Major faults of the northern Teruel Basin

The major faults in the northern Teruel Basin occur along the eastern, N-S trending active margin: El Pobo Fault Zone (EPFZ) and La Hita Fault Zone (LHFZ). Others are intra-basinal faults of diverse orientations and ages, several of them located at the junction with the Jiloca Graben: Tortajada, Peralejos, Concud, Teruel and Valdecebro faults (Fig. 2). In the following, we present the main features of these faults including the estimated total throw since the onset of the Teruel Graben, i.e. the vertical displacement of the *IES* planation level (11.2 Ma), as well as the post-*SEF* (3.5 Ma) throw.

The EPFZ represents the boundary of the Teruel Graben at its northern sector. It separates Neogene deposits from Mesozoic rocks of the El Pobo Range, giving rise to a 15 km-long mountain front trending N 175º E in average. In more detail the margin exhibits a zigzag pattern made of NNW-SSE trending, en-échelon arranged segments alternating with shorter N-S to NNE-SSW trending ones (Fig. 2). Individual faults are generally less than 1 km-long. A number of them, both synthetic and antithetic with the half-graben boundary, have been observed in outcrops, showing metre- to decamentre-scale offsets. Although scarce, slickenlines and other kinematic indicators show consistent normal movements. The total, post-Serravallian vertical displacement (*IES* marker) on the EPFZ is estimated to reach 1040 m, while that occurred since middle Pliocene time (*FES* marker) is 460-520 m (Fig. 3b). Displacement decreases northwards along the EPFZ (Fig. 3a). Together with the anthitetic intrabasinal Orrios Fault, the EPFZ bounds the subsident Escorihuela block where a continuous sedimentary series was deposited up to the Early Pleistocene (Ezquerro et al., 2012a,b; Rodríguez-López et al., 2012; Ezquerro, 2017).

The N-S trending LHFZ defines the central segment of the Teruel Basin margin; it is expressed in the landscape as an irregular mountain front separating the La Hita block from the Valdecebro depression (Fig. 2). At La Hita block, the *IES* and *FES* planation surfaces have an average altitute of 1640 m and 1500 m, respectively, while Ezquerro (2017) and Simón et al. (2018) locates these markers in the Valdecebro depression at 980 and 1250 m, respectively. Consequently, the total throw of LHFZ is estimated to 660 m, while the post-*FES* throw is about 250 m. North of this fault, a gentle monocline probably controlled by a N-S blind fault represented the diffuse basin margin until this was shifted to the Tortajada Fault (Fig. 3c).

The Tortajada Fault strikes NNE-SSW, separating the central sector of the Teruel Basin from the intermediate Corbalán block (Fig. 2). It was activated during the middle Turolian (Late Miocene, ca. 6.1 Ma), long after the overall Teruel Graben was set up (Ezquerro, 2017). From the geological cross section (Fig. 3c), its total throw is estimated at 350 m, while the post-*FES* throw approaches 260 m.

Towards NNE, a number of discontinuous fault traces (Peralejos Faults) apparently constitute the prolongation of the Tortajada Fault. The NNE-SSW trending, 8.5 km-long Peralejos Fault is made of NE-SW en échelon structures that extend up to obliquely abutting the EPFZ. Differently from the Tortajada Fault, the Peralejos Fault was activated since the onset of the Teruel Basin and therefore shows a higher displacement. From the altitude of *IES* and *FES* planation surfaces observed on the footwall block (1755 and 1560 m, respectively) and their position in the hanging wall block (720 and 1040 m, respectively; Fig. 3b), a total throw (post-*IES*) of ca. 1035 m, and a post-*FES* throw approaching 520 m have been estimated.

The Concud Fault is a NW-SE trending structure, whose recent average slip direction towards SW represents the negative inversion of a previous reverse, fold-related fault (Lafuente *et al*., 2011). It puts in contact Pleistocene alluvial deposits with Triassic and Jurassic units (western and central sectors), and with Neogene units of the Teruel Basin (southeastern sector), representing a junction structure between the Teruel and Jiloca grabens (Fig. 1). The accumulated net displacement for its overall extensional history (since latest Ruscinian, 3.5 Ma; Ezquerro, 2017) has been previously estimated by Lafuente et al. (2014) within the range of 255-300 m (throw = 240-280 m) based on the displacement of the top of the pre-tectonic stratigraphic level.

The Teruel Fault is an intra-basinal structure that shows a continuous N170ºE trending trace at the northern sector, while branches off southwards into two main fault traces trending N-S and NNW-SSE, respectively (Simón et al., 2017). It has accumulated a throw of ca. 250 m since 3.5 Ma, partially accommodated by bending at surface, with average slip direction towards N275ºE of its hanging wall block (Ezquerro, 2017; Simón et al., 2017). The Concud and Teruel faults make a right-stepping, 1.3-km-wide relay zone, while they show no structural link and behave as kinematically independent structures (Simón et al., 2017).

Finally, the Valdecebro Fault separates the Jurassic limestones of the upthrown Corbalán block from Miocene-Pliocene deposits of the Valdecebro depression. It is made of a number of extensional, both synthetic and antithetic ruptures striking E-W to ESE-WNW (Simón et al., 2018). It has undergone pure normal movement since Early Pliocene times (3.7 Ma), totalizing a throw of 190 m estimated from vertical offset of *FES* (Ezquerro, 2017; Simón et al., 2018).

5. Fracture patterns in Mesozoic and Neogene materials

The Mesozoic rocks of the eastern footwall blocks (from north to south, El Pobo Range, Cabigordo, and La Hita), the western basin margin (Palomera Range), and the intrabasinal highs (Santa Ana and Sierra Gorda) show a dense network of faults and fractures (Fig. 4). Fracture length ranges from several tens of metres to 6 km, and most of them (10,686 out of 12,666; 84%) are < 500 m in length. Only 49 fractures (0.4 %) are longer than 2 km. In a first approach, the rose diagram compiling directions of individual fractures (Fig. 5a) shows a wide dispersion, although an absolute maximum oriented NE-SW can be identified. In contrast, major faults (traces longer that 2 km) are distinctly oriented, prevailing those striking N-S and NNE-SSW (Fig. 5b). When the azimuth distribution is weighted according to fault length (Fig. 5c), four main sets can be distinguished: (i) NE-SW (range from 020º to 070º, with two relative maxima at 030º and 070º); (ii) E-W to ESE-WNW (090º–130º, with three relative maxima at 090º, 105º and 125º); (iii) N-S (170º–010º); and (iv) NNW-SSE (140º–160º). Fracture set (i) is widespread and homogeneously scattered all over the region, although it is denser between the latitudes of Teruel and Peralejos (Fig. 4). Fracture sets (ii), (iii) and (iv) have also been observed in all the sectors, but they are better developed in some specific areas (Fig. 4): the N-S set at the Corbalán and north of Cabigordo blocks, and the NNW-SSE and E-W to WNW sets northwards of the Alfambra latitude (El Pobo, Santa Ana and Palomera range blocks).

Faults and fractures in Neogene materials include the large structures creating the basin boundary as well as shorter intra-basinal faults, most of them close to the active margin (Fig. 4). Fracture length ranges from 10 m to 10 km, and most of them (1,782 out of 2,571; 69%) have lenghts < 500 m. A total of 76 Neogene fractures (3%, clearly higher than for Mesozoic ones) are > 2 km in length. In this case, the azimuth distribution, accounting both absolute number of fractures (Fig. 5d) and accumulated length (Fig. 5f) shows a clear maximum close to N-S (range 340º to 020º), although structures quite homogeneously distributed in the rest of directions also exist. Major faults (traces longer than 2 km) show two additional relative maxima around NE-SW and NW-SE (Fig. 5e). The N-S faults and fractures are mainly located at the eastern active margin, while the rest, especially those oriented NE-SW, are mainly distributed in intrabasinal positions. This fracture pattern differs from that described for Mesozoic materials, which allows inferring the true imprint of the Late Neogene, E-W extensional stress field in contrast with the Mesozoic inheritance, as discussed later.

6. Neogene stress fields

In a first approach, the predominance of nearly N-S striking faults in Neogene materials suggests that they could have been activated under an extensional stress field with σ_3 axes trending about E-W. In more detail, this stress field can be reconstructed using the abundant available regional literature (Simón, 1982, 1983, 1989; Paricio and Simón, 1986; Simón and Paricio, 1988; Cortés, 1999; Liesa, 2000, 2011a; Arlegui et al., 2005, 2006; Lafuente, 2011). Table 1 lists the ensemble of palaeostress results ascribed to the Neogene-Quaternary stress systems from those publications. It includes 55 sites mostly located in basinal Neogene-Quaternary sediments (50 sites), while the others lie in pre-Neogene rocks of the basin margin (Fig. 4). Information for each stress solution includes the number of explained faults, the total number of fault data, the orientation of stress axes and the stress ratio, the uncertainty expressed as average misfit angle between theoretical and measured slickenlines, as well as chronological relationships between stress states. In addition, Table 2 lists the results of the new 24 sites in Neogene deposits within the basin studied by Ezquerro (2017) in his unpublished PhD work; for each site, the stereoplot of fault orientations and stress axes representing the resulting stress state(s) is depicted in Figure 4.

We use the overall data for refining the regional stress evolution model during Late Neogene-Quaternary times in the central-northern sector of the Teruel Basin. Only 36 among the ensemble of fault sites contain fault planes with slickenlines, which were analysed following the above mentioned protocol based on *Rigth Dihedra,* Etchecopar's and *y-R* methods (Angelier and Mechler, 1977; Etchecopar et al., 1981; Simón, 1986). The remaining sites (43) had meso-scale fault planes showing small ofsets but no visible striations, these being analysed using the method proposed by Lisle et al. (2001). While the former sites could provide reliable stress orientations and stress ratios (R = $(\sigma_2 - \sigma_3) / (\sigma_1 - \sigma_3)$), the latter have not allowed acceptable constraint of R values. In the case of the non-striated fault planes studied by Ezquerro (2017), R values provided by the FSA software (Celérier, 2011) are included in Table 2, but their reliability is also weak.

The ensemble of palaeostress results on the Teruel Basin includes 58 complete deviatoric stress tensors, and 33 stress solutions for which the R ratio is unknown (Fig. 6). In almost all sites, the inferred σ_1 axis is nearly vertical, in agreement with the extensional character of the Neogene regional stress field. Only four stress tensors have horizontal σ_1 axis and, except for one, subvertical σ_2 axis, i.e. mainly representing strike-slip stress regimes. Accordingly, only the trend of the main principal horizontal axis (σ_3 in extensional regime and σ_1 in compressional or strike-slip ones) was compiled in Tables 1 and 2.

Several fault surfaces have two (exceptionally three) different striae generations. In general, the first set shows lower pitch than the second one, the latter being close to 90º and always exhibiting normal kinematics. Such cross-cut relationships between striae sets, together with the early or later deformational character of faulting, and the stress orientation in relation with bed attitude (pre- and post-tilting stress state; e.g. Simón, 1982, 1996; Angelier et al., 1985; Liesa and Simón, 2009) have been used for relatively dating palaeostress states in some sites (e.g. P6, P17, P19, P31, and P38 in Table 1, and sites 3, 9, 14, 15, and 23 in Table 2). Such chronological constraints are included in Tables 1 and 2 and graphically displayed (arrows) in Figure 6.

The four datasets characterized by a horizontal σ_1 have directions NNE-SSW and NNW-SSE to N-S (labelled as A and B, respectively, in Fig. 6a). Chronological constraints indicate that they likely acted prior to the extensional stress states, and that the NNE-SSW direction was prior to the N-S one (see arrows associated to sites 23 and P31 in Fig. 6a).

Concerning the direction of horizontal σ_3 axes in a purely tensile regime (R>1), the synthetic y-R diagram (Fig. 6a) and histograms (Fig. 6b,c) show their distribution for stress states affecting the Late Miocene-Quaternary sedimentary succession. The overall results show the predominance of σ_3 axes flipping around the E-W direction, although two maxima can be distinguished: an absolute maximum close to ENE-WSW (azimuth 055º-075º; label 1 in Fig. 6b), and a second, relative maximum close to E-W (085º-100º; label 2 in Fig. 6b). Other relative maxima can be observed around the directions NNE-SSW to NE-SW (030º-040º), NW-SE (120º-130º), and N-S (350º-000º) (labels 3, 4 and 5, respectively, in Fig. 6b).

If we consider the age of the deposits where such stress systems have been recorded (Fig. 6c), E-W σ_3 directions are dominant during Late Miocene-Early Pliocene (Turolian-Ruscinian), while ENE-WSW σ_3 directions are mainly recorded in Villafranchian-Pleistocene sediments (where the E-W extension is not represented). The other directions (maxima 3, 4 and 5) appear all along the stratigraphical series.

With respect to the spatial distribution of inferred extensional directions, the ENE-WSW (1) and E-W (2) are recorded all along the basin and related to different structural settings (Fig. 4). The other extensional directions (3, 4 and 5) are recorded at few localities trending either parallel or perpendicular to major structures. As an example, the NNE-SSW to NE-SW (3) and NW-SE (4) mainly appear near the NW-SE Concud Fault or the NE-SW Tortajada Fault. This suggests that they represent local deflections of stress trajectories, as those modellized by e.g., Simón et al. (1988) and Katternhorn et al. (2000), and identified by Simón (1989) and Arlegui et al. (2006) in this region.

Apart from the older compressional and strike-slip episodes, the Neogene stress field evolution has been therefore characterized from the whole analysis of the distribution of azimuths and R values of extensional stress states affecting the sedimentary sequence (Fig. 6), mesostructural evidence on their relative age (Tables 1, 2), and the heterogeneous spatial distribution of stress directions attributed to stress deflection (Fig. 4). The results suggest the occurrence of two major extensional stress episodes: (i) the first episode (Vallesian–Ruscinian or Tortonian–Zanclean in age) is characterized by a triaxial stress regime with well-defined σ_3 axes trending close to E-W; (ii) the second one (since early Villafranchian or Piancenzian) is characterized by almost radial extensional regime (σ_1 vertical, $\sigma_2 \approx \sigma_3$; very high R values). Although multiple σ_3 maxima are asigned to this second episode from the available dataset (as a consequence of stress deflection phenomena; see section 7.2), the overall regional results suggest that the ENE-WSW trending σ_3 axes represent its primary or remote stress system (Simón 1989; Arlegui et al., 2005). The chronological distribution of stress solutions depicted in Figure 6c also corroborates that the ENE-WSW extension direction prevails since Villafranchian time.

7. Discussion

7.1. Discerning structural inheritance

As a first approach, the differences observed between fracture patterns described for Mesozoic and Neogene rocks suggest: (i) the essential structural imprint of the Late Neogene, E-W and ENE-WSW oriented extensional stress systems is associated with the N-S trending fault set; (ii) the structural inheritance from ancient tectonic phases is mainly represented by NE-SW and E-W to ESE-WNW trending faults and fractures, and also probably by NNW-SSE ones.

Large (> 20 km) NNW-SSE trending, nearly vertical faults appear eastwards from the study area (e.g. Miravete, Alpeñés and Ababuj faults), most of them likely originated during

Variscan or late-Variscan tectonic phases (Soria, 1997; Liesa et al., 2006). These faults, together with newly formed, NE-SW to ENE-WSW striking, low angle listric faults, controlled the structural development and sedimentation of the Galve sub-basin during the Late Jurassic-Early Cretaceous rifting phase affecting eastern Iberia (Soria, 1997; Soria et al., 2000; Capote et al., 2002; Liesa et al., 2004, 2006; Navarrete et al., 2013). This rifting stage was responsible for the development of a dense fracture network at different scales, mainly affecting the prerift Jurassic carbonate rocks (as in the El Pobo Range) but also the synrift sediments of the Cretaceous Maestrazgo Basin (Liesa, 1992-1995, 1993, 2000, 2011a; Liesa and Simón, 1994; Antolín-Tomás et al., 2007). Based on the spatial distribution, changes in orientation, relative dimensions and cross-cut relationships of major faults, small-scale faults and joints in the El Pobo Range, Liesa (2000, 2011a) stated that they are arranged in two fractures systems. Each system consists of two orthogonal sets: the older sets are oriented NW-SE and NE-SW, while the younger ones trend N-S and E-W, respectively. A similar fracture network is expected to occur at the Jurassic basement of the Neogene Teruel Basin. During Palaeogene and Early Neogene times, most of those major faults underwent positive inversion under compressional stress fields linked to the Alpine orogeny; as a result, they controlled the position, style and evolution of most contractional structures (Simón et al., 1998; Liesa and Simón, 2004, 2011; Liesa et al., 2004).

In this way, the Neogene extension acted on an extremely heterogeneous Mesozoic-Cenozoic sedimentary cover, densely fractured during multiple tectonic episodes. Taking into account the stress regime and stress orientations characterizing each rifting episode, it could be deduced that: (i) the earlier, Late Miocene to Early Pliocene triaxial extension was the main responsible for reactivated or newly created faults, clustered around N-S trend; (ii) the later, Late Pliocene to Quaternary 'multidirectional' extension was able to reactivate such N-S trending faults as well as most previous, inherited fault sets of varying orientations.

A clear example of reactivation of a previous contractional structure is the case of the NW-SE Concud fault. This normal fault represents the southernmost structure of the Jiloca Basin (Fig. 1), which formed during the Late Pliocene and cut the sedimentary infill of the previous N-S Teruel Basin (e.g. Moissenet, 1983; Simón, 1983). This fault follows the near vertical to overturned limb of an NW-SE anticline with a Triassic core. This relation suggests that the Concud normal fault could represent the negative inversion of a reverse fault that developed (with an associated propagation fold) during the Palaeogene compresional stage. This interpretation was verified by Lafuente (2011) and Lafuente et al. (2011) when evinced (i) a hectometre-scale klippe of Triassic rocks over Jurassic ones at the central part of the fault trace, and (ii) a ductile shear band, contiguous and subparallel to the present-day normal fault, developed in Triassic lutites with an internal S-C fabric indicating a reverse-dextral movement.

The Teruel Basin itself could also represent the reactivation of a major NNE-SSW basement structure since it separates two sectors where the compressional structures show quite different strikes. The Jurassic intrabasinal highs and the western sectors of the basin show folds mainly trending NW-SE (Godoy et al., 1993a), while main folds in the eastern sector (the El Pobo Range and eastwards) trend NNW-SSE and have ENE-WSW superposed folds (Simón et al., 1998; Liesa, 2000, 2011b; Liesa et al., 2004). Such major crustal structure has been also proposed as responsible for deviating the σ_1 stress trajectories of the *Iberian* and *Betic* intraplate compressional stress fields during the Alpine Orogeny (Liesa, 2000; Capote et al., 2002; Liesa and Simón, 2007, 2009).

7.2 The dynamic framework: strain/stress partitioning within the Late Neogene-Quaternary stress field

The palaeostress results revealed here are consistent with the evolutionary model proposed by Simón (1982, 1983, 1989), in which two rift episodes control the development of Neogene basins in the eastern Iberian Chain. During the first episode, Late Miocene in age, the NNE-SSW trending Teruel and Maestrazgo grabens developed under a dominant E-W to ESE-WNW extension (Simón, 1982, 1986, 1989; Cortés, 1999; Capote et al., 2002; Liesa, 2011a). The second rift episode has been linked to crustal doming taking place in the eastern Iberian Chain during Late Neogene-Quaternary times (Simón, 1982, 1989). This hypothesis is supported by geophysical evidence on a negative density anomaly in the upper mantle of this region (Piromallo and Morelli, 2003; Boschi et al., 2010), which could have induced a positive dynamic topography of several hundred metres (Scotti et al., 2014). The resulting stress field is characterized by nearly 'multidirectional' tension with primary σ_3 trajectories trending ENE-WSW, giving rise to development of the NNW-SSE trending Jiloca gaben, the reactivation of most of the previous extensional margins, and pervasive deformation of the *Fundamental Erosion Surface* (Simón, 1982, 1989; Capote et al., 2002; Arlegui et al., 2005, 2006; Liesa, 2011a).

The regional stress fields active during both rift episodes show spatial heterogeneities. Within the overall available palaeostress database, secondary relative maxima of σ_3 axes at azimuths 350º–000º (labelled as 5 in Fig. 6), 030º–040º (3), and 120º–130º (4) should be interpreted in terms of stress deflections and stress swaps induced by major faults, mainly in the second, near multidirectional extensional episode. Such interpretation is based on the parallelism or orthogonality observed between some of these σ_3 directions (mainly for 350º–000º and 030º–040º ones) and some of the major faults (e.g. sites P33 and P36 with respect to EPFZ; sites 10, 11, 17-20 and 21 with respect to Peralejos and Tortajada faults; or sites P19, P20, P28, P30, P42 and 21 with respect to the Concud Fault; Fig. 4). Minor-order stress heterogeneities are frequent within 'radial' or 'multidirectional' tension stress fields. First, trajectories of the minimum stress axis (σ_3) undergo frequent deflections, veering to become either parallel or perpendicular to NNW-SSE and NNE-SSW major faults, which follow the numerical models of stress deflections (e.g. Simón et al., 1988; Kattenhorn et al., 2000). A progressive variation of the shape of stress ellipsoids, from near-multidirectional to triaxial tension, frequently accompanies such deflection as approaching active faults (Arlegui et al., 2006). Second, swap events between σ_2 and σ_3 axes are also common phenomena in the region (Simón et al., 1988; Simón, 1989), which can explain the occurrence of both joint sets and conjugate normal fault systems striking at right angles to the master faults.

Concerning the timing of stress systems, the results summarised in Figure 6c suggest that the transition between stress systems associated to both rift episodes possibly occurred close to the Ruscinian-Villafranchian boundary. Nevertheless, both E-W to ESE-WNW, and ENE-WSW extension directions have been recorded within the Miocene-Pliocene series. This suggests that they do not strictly represent two successive tectonic phases, but separation of the extensional stress field into two stress systems, with S_{Hmax} (maximum horizontal stress axis) nearly parallel to the trends of the Teruel and Jiloca grabens, respectively. Moreover, such S_{Hmax} directions replicate the main far-field stresses acting during the Neogene-Quaternary in eastern Spain: the intraplate NNW-SSE compression produced by Africa-Iberia convergence, and the WNW-ESE extension induced by rifting at the Valencia trough (Simón, 1989; Herraiz et al., 2000; Capote et al., 2002; Arlegui et al., 2005). Such stress setting has been defined by Simón *et al.* (2008) as *stress partitioning*, i.e. 'time dissociation' of the overall stress field into distinct genetic stress systems similar to that described in the Italian Alps as *Twist Tectonics* by Caputo et al. (2010). In accordance with the above explained processes, progressive deformation occurs in the form of a non-linear succession of fracture episodes; each of them is controlled by stress boundary ('*Andersonian*') conditions, while the ensemble of them finally accommodates triaxial bulk deformation of the rock body (Simón et al., 2008).

Partitioning of the Neogene-Quaternary stress/strain field in Eastern Iberia is a consequence of both the complex tectonic framework and the influence of inherited structures.

The WNW-ESE extension active by the Late Miocene is linked to rifting at the Valencia Trough (Simón, 1982), but it is also coaxial with the later *Pyrenean compression* (maximum horizontal stress, S_{Hmax} trending NNE-SSW), as defined by Liesa (2000), Capote et al. (2002) and Liesa and Simón (2007, 2009). The WSW-ENE extension that dominates during Late Pliocene and Quaternary times reveals the presence of NNW-SSE trending S_{Hmax} trajectories (maximum horizontal stress) controlled by the recent Iberia-Africa convergence (Simón, 1989; Herraiz et al., 2000; Arlegui et al., 2005). Both tectonic mechanisms coexist during the whole Neogene and Quaternary, and both extension directions, WNW-ESE and WSW-ENE, are recurrently recorded during this time lapse indeed (Cortés et al., 1996; Arlegui and Simón, 2000; Arlegui et al., 2005). Episodic 'inhibition' of one of them owing to stress release subsequent to fault movement may allow the second one to be manifested (Simón et al., 2008). They can be therefore recorded as separate stress states in different areas within the whole region (spatial stress partitioning) as well as in different time windows within the whole tectonic period (temporal stress partitioning).

Such dissociation of stress systems was facilitated by the existence of diverse inherited fault sets. Once these faults were progressively propagated, the successive stress systems selectively activated those favourably oriented. Slip on master structures controlling Neogene grabens probably accommodated most of the total deformation, i.e. NNE-SSW faults driven by rifting at the Valencia Trough, and NW-SE to NNW-SSE faults born as contractional structures during Palaeogene orogeny, then inverted during Neogene rifting. But the whole region (specifically, the El Pobo Range and Alfambra depression) shows other multiple fault sets (most of them inherited from Mesozoic extensional episodes; Liesa, 2000, 2011b). The ensemble of them provided the best possible conditions for stress-strain partitioning, mainly during the later 'multidirectional' extensional episode.

7.3. The resulting zigzag basin margin and intrabasinal deformation

As a result of fault linkage within the described structural and dynamic ascenario, the eastern margin of the northern Teruel Basin acquired a zigzag arrangement at the same time as the intrabasinal structure was getting more and more complex. In homogeneous and isotropic materials, evolution of relay zones up to accomplish linkage uses to follow its own kinematic rules, essentially controlled by the relationship between geometry, transport direction and interaction of master faults (e.g. Cartwright et al., 1995; Gupta and Scholz, 2000). By contrast, in more complex tectonic settings inherited structures and their response to stress are the main controls of fault linkage and margin arrangement, as well as of intrabasinal deformation.

In the northernmost sector of the Teruel Basin, the orientation of faults that control the alternating N-S to NNE-SSW, and NNW-SSE trending segments (Fig. 7) coincide with the two main directions of large-scale faults (L > 2 km) cutting Mesozoic rocks. Moreover, both fault directions are nearly orthogonal to the σ_3 trajectories of the prevailing stress systems: E-W to ESE-WNW (earlier extensional episode), and ENE-WSW (later extensional episode). Therefore, in this case, a dynamic scenario based on successive episodes of reactivation of pre-existing faults under favourable stress conditions provides a more feasible explanation for fault linkage than a scenario only controled by fault interaction. Based on tectono-sedimentary relationships at the short segments of the northernmost, zigzag arranged, EPFZ, Ezquerro (2017) has demonstrated how NNW-SSE trending segments developed prior to the N-S to NNE-SSW trending ones. Such sequence of fault episodes in those distinctly oriented segments is the opposite to the regional rifting sequence, and are constrained to the second rift episode (Ruscinian-Villafranchian; Ezquerro, 2017). This suggets that we are not properly dealing with successive stress episodes, but with a typical case of space–time stress partitioning (Caputo, 2005). Their interpretation is that NNW-SSE striking faults were firstly activated under ENE-WSW extension characterizing the Late Pliocene stress field. Subsequently, local perturbation related to interaction between neighbouring faults produced a slight change of the stress trajectories, the σ_3 direction flipping to E-W or ESE-WNW and thus triggering activation of NNE-SSW segments. In this way, two successive stress episodes, representing both time and space partitioning of the regional stress field (Simon et al., 2008), have resulted in a somewhat orthorombic or 'biconjugate' fault system that accommodates three-dimensional bulk deformation (Reches, 1978; Reches and Dieterich, 1983; Crider and Pollard, 1998).

On the basis of the presented data, a similar situation can be envisaged for the ensemble of the central-northern sector of the Neogene Teruel Basin (Fig. 8). Accordingly, we propose a scenario in which the evolving extensional stress system was able to gradually activate major basement structures of variable direction inherited from previous deformational stages, then controlling the structure and evolution of both the margin and central parts of the basin. Timing and amplitude of fault displacements are constrained from throws measured on the successive sedimentary units as well as on the planation surfaces, *IES* (11.4 Ma) and *FES* (3.5 Ma). The combined use of such sedimentary and geomorphological markers allow reconstructing the timing of both intrabasinal and boundary master faults. Roughly N-S to NNE-SSW trending, eastern border faults (e.g. the EPFZ (south sector) and LHFZ and the Peralejos Faults) frequently record significant displacements during the Late Miocene (post-*IES* to pre-*FES*), as much as in recentmost times (post-*FES*). Intrabasinal faults of variable direction, however, show a much lower (Tortajada, Teruel, and Valdecebro faults) or null (Concud fault) displacement in the first stage, whereas they undergo higher activity in more recent times.

Accordingly, Figure 8 shows an evolutionary model in two stages. The overall Teruel Graben was onset at the beginning of the Late Miocene (~ 11.2 Ma), when the N-S fault zones of its eastern margin (La Hita and El Pobo) were activated within an E-W to ESE-WSW triaxial extension. The LHFZ likely continued northwards as a blind structure, as suggested by the aligned N-S trending monocline observed at the Cabigordo block (Fig. 3c) and the high vertical offset pre-*FES* associated to it (Ezquerro, 2017). In addition, the Peralejos Fault interposed between the two major fault zones also recorded high displacements. At this stage, this NE-SW trending structure represented a long linking zone between EPFZ and LHFZ, where NNE-SSW segments were reactivated to form a NE-SW trending right-stepping relay setting. During the Late Pliocene (~ 3.5 Ma), when the remote extensional stress regime became almost radial ($\sigma_2 \approx \sigma_3$) though with a prevailing ENE-WSW tensile direction, the former structures remained active while other faults of variable direction were reactivated mainly in intrabasinal sector. Northward propagation of the EPFZ also occurred in this second stage, after development of the *FES* planation level (Ezquerro, 2017). The transition between both stages likely occurred in a progressive manner, as suggested by the onset of the NNE-SSW Tortajada Fault during the middle Turolian (Late Miocene, ca. 6.1 Ma). In its hangingwall, sediments of this age have reworked clasts of Neogene conglomerates sourced at the Corbalán footwall block (Ezquerro, 2017).

The above described intrabasinal and bordering fault network of the Teruel Basin is more complex than those normaly displayed in other intracontinental rift basins (e.g. Basin and Range in USA or East African rift system), where more linear structures (rift valleys) are present. As it has been shown, such complex structure of the central-northern Teruel Basin was clearly controlled by both the variable orientation of inherited structures and the evolving, Late Miocene to Quaternary regional stress field. Active processes in central-eastern Iberia changed in time due to the complex plate kinematics of the relatively small Iberian plate and the neighbouring Europe and Africa major plates. Intraplate deformation was strongly influenced by the evolving interaction between the stress systems mainly transmitted from the plate boundaries, i.e. the remained NNE-SSW Iberia-Europe convergence, the NNW-SSE Africa-Iberia convergence, the E-W active extension in the eastern Valencia Trough, and the crustal doming process during Pliocene-Quaternary times.

8. Conclusions

Two distinct episodes can be distinguished during the evolution of the Teruel Basin: (i) an ealier episode (Late Miocene-Early Pliocene in age) characterized by triaxial extension with σ_3 trajectories close to E-W, and (ii) a later episode (Late Pliocene-Quaternary) with prevailing ENE-WSW trending σ_3 trajectories though characterized by an almost radial extensional regime.

The earlier stress episode was responsible for the onset of the northern Teruel half-graben and propagation of a major, N-S trending set of newly formed faults. Nevertheless, a dense network made of NNE-SSW and NNW-SSE striking segments, mostly consisting of inherited Mesozoic fractures, also contributed to the development of the eastern basin margin. Mainly at its northernmost sector, early linkage through narrow fault relay zones enabled prompt development of a zigzag arrangement (Fig. 7). These faults were selectively reactivated under the E-W extensional stress field (a process usually easier than the formation of new faults), and remain as well active during the second stress episode.

At the central sector of the basin, activation of faults of other diverse orientations (Concud, NW-SE; Tortajada, NE-SW; Valdecebro, E-W), resulted in a more complex structural network. Such activations also occurred during the second stress episode, during which ‘radial’ extensional deformation should be necessarily accommodated by a variety of fault sets.

Both structural inheritance and deformational processes (especifically the remote and driving stress systems) appear as first-order factors in the resulting structure and evolution of rift basins because they ultimately control whether inherited or newly-formed structures will developed.

Acknowledgements

We wish to acknowledge the thorough reviews and valuable comments of Kieran F. Mulchrone and Riccardo Caputo. We want to extend our appreciation to Editor Joao Hippertt for taking the time and necessary effort to help in the improvement of this work. The research has been financed by projects CGL2012-35662 of Spanish Ministerio de Economía y Competitividad-FEDER, and UZ2017-CIE-01 of Universidad de Zaragoza. This work is a contribution of the *Geotransfer* research group, co-financed by the Aragón Government and the PO FEDER Aragón 2014-2020.

References

Alcalá, L., Alonso-Zarza, A.M., Álvarez, M.A., Azanza, B., Calvo, J.P., Cañaveras. J.C., van Dam, J.A., Garcés, M., Krijgsman, W., van der Meulen, A.J., Morales, J., Peláez, P., Pérez-González, A., Sánchez, S., Sancho, R., Sanz, E., 2000. El registro sedimentario y faunístico de las cuencas de Calatayud-Daroca y Teruel. Evolución paleoambiental y paleoclimática durante el Neógeno. Revista de la Sociedad Geológica de España 13, 323-343.

Alonso-Zarza, A.M., Calvo, J.P., 2000. Palustrine sedimentation in an episodically subsiding basin: the Miocene of the Northern Teruel Graben (Spain). Palaeogeography, Palaeoclimatology, Palaeoecology 160, 1-21.

Álvaro, M., Capote, R., Vegas, R., 1979. Un modelo de evolución geotectónica para la Cadena Celtibérica. Acta Geológica Hispánica 14, 172-177.

Angelier, J., Mechler, P., 1977. Sur une méthode graphique de recherche des contraintes principales également utilisable en tectonique et en séismologie: la méthode des dièdres droits. Bulletin de la Societè Géologique de France 19, 1309–1318.

Angelier, J., Colleta, B., Anderson, R.E., 1985. Neogene paleostress changes in the Basin and Range: A case study at Hoover Dam, Nevada-Arizona. Geological Society of America

Bulletin 96, 347-361.

Antolín-Tomás, B., Liesa, C.L., Casas, A.M., Gil-Peña, I., 2007. Geometry of fracturing linked to extension and basin formation in the Maestrazgo basin (Eastern Iberian Chain, Spain). Revista de la Sociedad Geológica de España 20, 351-365.

Arlegui, L.E., Simón, J.L., 2000. Fracturación y campos de esfuerzos en el Cuaternario del sector central de la Cuenca del Ebro (NE España). Cuaternario y Geomorfología 14, 11-20.

Arlegui, L.E., Simón, J.L., Lisle, R.J., Orife, T., 2005. Late Pliocene-Pleistocene stress field in the Teruel and Jiloca grabens (eastern Spain): contribution of a new method of stress inversion. Journal of Structural Geology 27, 693-705.

Arlegui, L.E., Simón, J.L., Lisle, R.J., Orife, T., 2006. Analysis of non-striated faults in a recent extensional setting: the Plio-Pleistocene Concud fault (Jiloca graben, eastern Spain). Journal of Structural Geology 28, 1019-1027.

Boschi, L., Faccenna, C., Becker, T. W., 2010. Mantle structure and dynamic topography in the Mediterranean Basin. Geophysical Research Letters 37, doi: 10.1029/2010GL045001.

Bott, M.H.P., 1959. The mechanics of oblique slip faulting. Geological Magacine 96, 109-117.

Capote, R., Muñoz, J.A., Simón, J.L., Liesa, C.L., Arlegui, L.E., 2002. Alpine tectonics I: The Alpine system north of the Betic Cordillera. In: Gibbons, W., Moreno, T. (Eds.) Geology of Spain, The Geological Society, London. 367-400.

Caputo, R., 2005. Stress variability and brittle tectonic structures. Earth Science Reviews 70, 103-127.

Caputo, R., Poli, M.E., Zanferrari, A., 2010. Neogene–Quaternary tectonic stratigraphy of the eastern Southern Alps, NE Italy. Journal of Structural Geology 32, 1009–1027.

Cartwrigth, J.A., Trudgill, B.D., Mansfield, C.S., 1995. Fault growth by segment linkage: an explanation for scatter in maximum displacement and trace length data from the Canyonlands Graben of S.E. Utah. Journal of Structural Geology 17, 1319–1326.

Casas, A.M., Gil, I., Simón, J.L., 1990. Los métodos de análisis de paleoesfuerzos a partir de poblaciones de fallas: sistemática y técnicas de aplicación. Estudios Geológicos 46, 385-398.

Celérier, B., 2011. FSA: Fault, Stress Analysis software, version 33.7. http://www.pages-perso-bernard-celerier.univ-montp2.fr/software/dcmt/fsa/fsa.html

Cortés, A.L., 1999. Evolución tectónica reciente de la Cordillera Ibérica, Cuenca del Ebro y Pirineo centro-occidental. Ph.D. Thesis. University of Zaragoza, Zaragoza, pp. 409.

Cortés, A.L., Liesa, C.L., Simón, J.L., Casas. A.M., Maestro, A., Arlegui, L.E., 1996. El campo de esfuerzos compresivo neógeno en el NE de la Península Ibérica. Geogaceta 20, 806-809.

Crider, J.G., Pollard, D.D., 1998. Fault linkage: Three dimensional mechanical interaction between echelon normal faults. Journal of Geophysical Research 103, 24 373–24 324

Etchecopar, A., Vasseur, G., Daignières, M., 1981. An inverse problem in microtectonics for the determination of stress tensors from fault striation analysis. Journal of Structural Geology 3, 51–65.

Ezquerro, L., 2017. El sector norte de la cuenca neógena de Teruel: tectónica, clima y sedimentación. Ph.D. Thesis, University of Zaragoza, Zaragoza, pp. 494 p.

Ezquerro, L., Luzón, M.A., Liesa, C.L., Simón, J.L., 2012a. Evolución megasecuencial del relleno mio-plioceno del sector norte de la cuenca de Teruel: interacciones entre tectónica y sedimentación. In: Fernández, L.P., Fernández, A., Cuesta, A., Bahamonde, J.R. (Eds.) GeoTemas 13, Resúmenes extendidos del VIII Congreso Geológico de España, 171-174.

Ezquerro, L., Lafuente, P., Pesquero, Mª.D., Alcalá, L., Arlegui, L.E., Liesa, C.L., Luque, L., Rodríguez-Pascua, M.A., Simón, J.L., 2012b. Una cubeta endorreica residual plio-pleistocena en la zona de relevo entre las fallas de Concud y Teruel: implicaciones paleogeográficas. Revista de la Sociedad Geológica de España 25, 157-175.

Godoy, A., Olivé, A., Moissenet, E., Gutiérrez Elorza, M., Aguilar, M.J., Ramírez, J.I., Aragonés, E., Giner, J., Portero, J.M., 1983a. Mapa Geológico de España 1:50.000, hoja nº 542 (Alfambra). IGME, Madrid.

Godoy, A., Ramírez, J.I., Olivé, A., Moissenet, E., Aznar, J.M., Aragonés, E., Aguilar, M.J., Ramírez del Pozo, J., Leal, M.C., Jerez Mir, L., Adrover, R., Goy, A., Comas, M.J., Alberdi, M.T., Giner, J., Gutiérrez Elorza, M., Portero, J.M., Gabaldón, V., 1983b. Mapa Geológico de España 1:50.000, hoja nº XXX (Teruel). IGME, Madrid.

Gupta, S., Scholz, C.H., 2000. A model of normal fault interaction based on observations and theory. J. Struct. Geol. 22, 865-880.

Gutiérrez, M., Peña, J.L., 1976. Glacis y terrazas en el curso medio del río Alfambra (provincia de Teruel). Boletín Geológico y Minero 87, 561-570.

Herraíz, M., De Vicente, G., Lindo, R., Giner, J., Simón, J.L., González, J.M., Vadillo, O., Rodríguez, M.A., Cicuéndez, J.I., Casas, A., Rincón, P., Cortés, A.L., Lucini, M., 2000. The recent (Upper Miocene to Quaternary) and present tectonics stress distributions in the Iberian Peninsula. Tectonics 19, 762-786.

Homberg, C., Hu, J.C., Angelier, J., Bergerat, F., Lacombe, O., 1997. Characterization of stress perturbations near major fault zones: Insights from 2-D distinct-element numerical modelling and field studies (Jura mountains). Journal of Structural Geology 19, 703-718.

Katterhorn, S.A., Aydin, A., Pollard, D.D., 2000. Joints at high angles to normal fault strike: an explanation using 3-D numerical models of fault-perturbed stress fields. Journal of Structural Geology 22, 1-23.

Lafuente, P., 2011. Tectónica activa y paleosismicidad de la falla de Concud (Cordillera Ibérica central). Ph.D. Thesis. University of Zaragoza, Zaragoza.

Lafuente, P., Arlegui, L.E., Liesa, C.L., Simón, J.L., 2011. Paleoseismological analysis of an intraplate extensional structure: the Concud fault (Iberian Chain, Spain).). International Journal of Earth Sciences 100, 1713–1732.

Larroque, J.M., Laurent, P., 1988. Evolution of the stress field pattern in the south of the Rhine Graben from the Eocene to the present. Tectonophysics 148, 41-58.

Liesa, C.L., 1992-1995. Estudio de la fracturación de las rocas a distintas escalas en campos de esfuerzos complejos en Mosqueruela y la Sierra de Camarena (provincia de Teruel). Teruel 83-84, 31-80.

Liesa, C.L., 1993. Análisis de la deformación frágil en las áreas de Mosqueruela y La Puebla de Valverde (Teruel): fases tectónicas y perturbaciones de esfuerzos. Unpublised Tesis de Licenciatura, Univ. of Zaragoza, Zaragoza, pp. 98.

Liesa, C.L., 2000. Fracturación y campos de esfuerzos compresivos alpinos en la Cordillera Ibérica y el NE peninsular. Ph.D. Thesis. University of Zaragoza, Zaragoza, pp. 760.

Liesa, C.L., 2011a. Fracturación extensional cretácica en la Sierra del Pobo (Cordillera Ibérica, España). Revista de la Sociedad Geológica de España 24, 31-48.

Liesa, C.L. 2011b. Evolución de campos de esfuerzos en la Sierra del Pobo (Cordillera Ibérica, España). Revista de la Sociedad Geológica de España 24, 49-68.

Liesa, C.L., Simón, J.L., 1994. Fracturación a distintas escalas y campos de esfuerzos durante la tectogénesis alpina en el área de Mosqueruela (Teruel). Estudios Geológicos 50, 47-57.

Liesa, C.L., Simón, J.L., 2004. Modelos de inversión positiva en sistemas de fallas en graderío: los márgenes de las cuencas extensionales cretácicas en la Cordillera Ibérica centro-oriental. Geotemas 6, 229-232.

Liesa C.L., Simón, J.L., 2007. A probabilistic approach for identifying independent remote compressions: The case of the Iberian Chain (NE Spain). Mathematical Geology 39, 337-348.

Liesa, C.L., Simón, J.L., 2009. Evolution of intraplate stress fields under multiple compressions: The case of the Iberian Chain (NE Spain). Tectonophysics 474, 144-159.

Liesa, C.L.; Casas, A.M.; Soria, A.R.; Simón, J.L.; Meléndez, A. (2004) Estructura extensional cretácica e inversión terciaria en la región de Aliaga-Montalbán. In: Colombo, F., Liesa, C.L., Meléndez, A., Pocoví, A., Sancho, C., Soria, A.R. (Eds.) Itinerarios Geológicos por Aragón, Sociedad Geológica de España, Zaragoza. Geo-Guías 1, 151-180.

Liesa, C.L.; Soria, A.R.; Meléndez, N., Meléndez, A., 2006. Extensional fault control on the sedimentation patterns in a continental rift basin: El Castellar Formation, Galve sub-basin, Spain. Journal of the Geological Society, London 163, 487-498.

Lisle, R.J., Orife, T. Arlegui, L.E., 2001. A stress inversion method requiring only fault slip sense. Journal of Geophysical Research 106 (B2), 2281-2289.

Moissenet, E., 1983. Aspectos de la Neotectónica en la fosa de Teruel. In: Comba, J.A. (Ed.), Geología de España. Libro Jubilar J.M. Ríos, Vol. II. IGME. Madrid. 427-446.

Navarrete, R., Liesa, C.L., Soria, A.R., Rodríguez-López, J.P., 2013. Actividad de fallas durante el depósito de la Formación Camarillas (Barremiense) en la subcuenca de Galve (E de España). Geogaceta 53, 61–64.

Paricio, J., Simón, J.L., 1986. Aportaciones al conocimiento de la compresión tardía en la Cordillera Ibérica oriental: la cuenca neógena inferior del Mijares (Teruel-Castellón). Estudios Geológicos 42, 307-319.

Peacock, D.C.P., Sanderson, D.J., 1991. Displacements, segment linkage and relay ramps in normal fault zones. Journal of Structural Geology 13, 721–733.

Peña, J.L., Gutiérrez, M., Ibáñez, M.J., Lozano, M.V., Rodríguez, J., Sánchez-Fabre, M., Simón, J.L., Soriano, M.A., Yetano, L.M., 1984. Geomorfología de la provincial de Teruel, Instituto de Estudios Turolenses, 149 p.

Piromallo, C., Morelli, A., 2003. P-wave tomography of the mantle under the Alpine-Mediterranean area. Journal of Geophysical Research 108 (B2), doi:10.1029/2002JB001757.

Reches, Z., 1978. Analysis of faulting in three-dimensional strain fields. Tectonophysics 47, 109-129.

Reches, Z., Dieterich, J.H., 1983. Faulting of rocks in three-dimensional strain fields. I. Failure of rocks in polyaxial, servo-control experiments. Tectonophysics 95, 111-132.

Rispoli, R., 1981. Stress fields about strike-slip faults inferred from stylolites and tension gashes. Tectonophysics 75, 29–36.

Roca, E., Guimerà, J., 1992. The Neogene structure of the eastern Iberian margin: structural constraints on the crustal evolution of the Valencia trough (western Mediterranean). Tectonophysics 203, 203-218.

Rodríguez-López, J.P., Liesa, C.L., van Dam, J., Lafuente, P., Arlegui, L., Ezquerro, L., de Boer, P.L., 2012. Aeolian construction and alluvial dismantling of a fault-bounded intracontinental aeolian dune field (Teruel Basin, Spain); a continental perspective on late Pliocene climate change and variability. Sedimentology 59, 1536-1567.

Rubio, J.C., Simón, J.L., 2007. Tectonic subsidence v. erosional lowering in a controversial intramontane depression: the Jiloca basin (Iberian Chain, Spain). Geological Magazine 144, 1-15.

Scotti, V.N., Molin, P., Faccenna, C., Soligo, M., Casas-Sainz, A., 2014. The influence of surface and tectonic processes on landscape evolution of the Iberian Chain (Spain): Quantitative geomorphological analysis and geochronology. Geomorphology 206, 37-57.

Simón, J.L., 1982. Compresión y distensión alpinas en la Cadena Ibérica oriental. Ph.D. Thesis. Publ. Inst. Estudios Turolenses, Teruel.

Simón, J.L., 1983. Tectónica y neotectónica del sistema de fosas de Teruel. Teruel 69, 21-97.

Simón, J.L., 1986. Analysis of a gradual change in stress regime (example from the eastern Iberian Chain, Spain). Tectonophysics 124, 37–53.

Simón, J.L., 1989. Late Cenozoic stress field and fracturing in the Iberian Chain and Ebro Basin. Journal of Structural Geology 11, 285-294.

Simón, J.L., Paricio, J., 1988. Sobre la compresión neógena en la Cordillera Ibérica. Estudios Geologicos 44, 271-283.

Simón, J.L., Soriano, M. A. (1993). La falla de Concud (Teruel): actividad cuaternaria y régimen de esfuerzos asociado. In: Aleixandre, T., Pérez González, A. (Eds.), El Cuaternario de España y Portugal. ITGE, Madrid 2, 729-737.

Simón, J.L., Arenas, C., Arlegui, L., Aurell, M., Gisbert, P., Gonzalez, A., Liesa, C., Martin, C., Melendez, A., Melendez, G., Pardo, G., Soria, A.R., 1998. Guía del parque geológico de Aliaga. Ayuntamiento de Aliaga, Centro para el Desarrollo del Maestrazgo, Departamento de Geologia de la Universidad de Zaragoza.

Simón, J.L., Arlegui, L.E., Liesa, C.L., Maestro, A., 1999. Stress perturbations registered by jointing near strike-slip, normal, and reverse faults: Examples from the Ebro Basin, Spain. Journal of Geophysical Research (Solid Earth) 104, 15141-15153.

Simón, J.L., Arlegui, L.E., Liesa, C.L. (2008) Stress partitioning: a practical concept for analysing boundary conditions of brittle deformation. Geodinamica Acta 21, 107-115.

Simón, J.L., Arlegui, L.E., Lafuente, P., Liesa, C.L., 2012. Active extensional faults in the central-eastern Iberian Chain, Spain. Journal of Iberian Geology 38, 127-144.

Simón, J.L., Arlegui, L.E., Ezquerro, L., Lafuente, P., Liesa, C.L., Luzón, A., 2017. Assessing interaction of active extensional faults from structural and paleoseismological analysis: The Teruel and Concud faults (eastern Spain). Journal of Structural Geology 103, 100–119.

Simón, J.L., Liesa, C.L., Arlegui, L.E., Ezquerro, L., Luzón, A., Medialdea, A., 2018. Paleoseismicity of the Valdecebro fault (Teruel basin, Iberian Chain). In: Canora, C. (Ed.). Avances en el estudio de fallas activas, terremotos y peligrosidad sísmica de Iberia. III Reunión Ibérica sobre Fallas Activas y Paleosismología, Alicante (España), 115–118.

Soria, A.R., 1997. La sedimentación en las cuencas marginales del surco ibérico durante el Cretácico Inferior y su control tectónico. Ph.D. Thesis, University of Zaragoza, Zaragoza, pp. 363.

Soria, A.R., Meléndez, M.N., Meléndez, A., Liesa, C.L., Aurell, M., Goméz Fernández, J.C., 2000. The Early Cretaceous of the Iberian Basin (Northeastern Spain). In: Gierlowski-Kordesch, E.H. and, Kelts, K.R. (Eds.). Lake basins through space and time, AAPG studies in Geology 46, 285-294.

Walsh, J.J., Watterson, J., Bailey, W.R., Childs, C., 1999. Fault relays, bends and branch-lines. Journal of Structural Geology 21, 1019–1026.

Weerd, A., 1976. Rodent faunas of the Mio-Pliocene continental sediments of the Teruel-Alfambra region, Spain. Ph.D. Thesis. Utrecht Micropaleontol. Bulletin, Special Publication 2. Utrecht.

FIGURE CAPTIONS

Fig. 1. (a) Location of the northern Teruel Basin within the eastern Iberian Peninsula. (b) Overall cross section of the northern Teruel half-graben.

Fig. 2. Synthetic structural map of the northern Teruel Basin showing the main faults at its eastern margin, as well as the prerift blocks cropping out in the eastern and western basin margins and in intrabasinal locations.

Fig. 3. Geological cross-sections along the northern sector of the Teruel Graben (see location in Figure 2). Fault throws are estimated from the *IES* and *FES* planation surfaces markers.

Fig. 4. Detailed map of fracture systems in Neogene and Mesozoic units in and around the central-northern Teruel Basin. Stereoplots represent fault orientations and stress axes obtained by Ezquerro (2017). Blue arrows indicate the azimuth of the σ_3 axis of extensional stress tensors. Red arrows indicate the azimuth of the σ_1 axis of compresional stress tensors. Numbers close to black dots refer to literature data (see Table 1), while those in white small circles refer to Table 2 (Ezquerro, 2017).

Fig. 5. Frequency distribution of fracture directions in and around the central-northern Teruel Basin. (a), (b), (c): fractures in Mesozoic units. (d), (e), (f): fractures in Neogene units. Histograms represent accumulated fracture lengths for classes of 1º; the smoothed frequency curve (rolling average and window of 10º) is also shown. Rose diagrams represent the absolute number of fractures for classes of 10º, and they are elaborated for both the total fracture population and map-scale, > 2 km-long faults.

Fig. 6. Distribution of palaeostress directions (mainly tensile stress tensors) recorded in the central-northern Teruel Basin. (a) Synthetic y-R diagram of stress tensors for which the R stress ratio is available; the blue shadow displays the main clusters of horizontal σ_y azimuts ($\sigma_y = S_{Hmax}$ = maximum horizontal stress, corresponding to σ_2 in all cases); $R = (\sigma_z - \sigma_x) / (\sigma_y - \sigma_x)$, Bott

(1959). (b) Histogram of total σ_3 azimuts recorded along the Late Miocene-Quaternary series, including those stress solutions with (in green) and without (in blue) R stress ratio; vertical pink bands correlate the relative maxima that are tentatively interpreted as the prevailing recent stress systems, as discussed in the text. (c) Separated histograms of σ_3 azimuts and chronological relationships according to the age of rocks where they are recorded.

Fig. 7. Detail of the zigzag fault arrangement of the northern El Pobo Fault Zone (EPFZ) (see Fig. 2 for location).

Fig. 8. Sketch showing the general evolution of the central-northern sector of the Neogene Teruel Basin. EPFZ: El Pobo Fault Zone; PF: Peralejos Fault; TF: Tortajada Fault; VFZ: Valdecebro Fault Zone; LHFZ: La Hita Fault Zone; TeF: Teruel Fault; CF: Concud Fault; SPFZ: Sierra Palomera Fault Zone.

TABLE CAPTIONS

Table 1. Palaeostress results compiled from previous publications. 1: Lafuente (2011), 2: Arlegui et al. (2006), 3: Simón (1989), 4: Arlegui et al. (2005), 5: Liesa (2011), 6: Cortés (1999), 7: Simón and Paricio (1988). Extensional and compressional stress tensors are distinguished. The following information is given for each data site: acronym used in the present work, in particular in Figure 4; name or acronym from the original publication; UTM coordinates, X and Y; affected rocks (Lm: limestone, Gy: gypsum, Mu: mudstone, St: sandstone, Co: conglomerate); age; lithostratigraphic unit according to Godoy et al. (1983a,b) (CL: Cuevas Labradas Fm., UDI: *Unidad Detrítica Inferior-Rojo 1*, CI: *Calizas Intermedias*, P1: *Páramo 1*, P2: *Páramo 2*, R3: *Rojo 3*, VP: *Villafranchian Pediment*); genetic unit according to Ezquerro (2017); azimuth of the horizontal σ_3 axis (extensional tensors) or the horizontal σ_1 axis (compressional tensors); stress ratio R_e used by Etchecopar et al. (1981); stress ratio R used by Bott (1959); (1), (2), (3) indicate chronological order of stress tensors; mean *angular misfit* (º) between observed slip and the

resolved shear stress from the computed stress solution; number of explained faults (n) in relation with the total number of faults of the site, and analytical method used for stress inversion (ET: Etchecopar's method, yR: y-R diagram method, Li: Lisle et al. (2001) method).

Table 2. Palaeostress results obtained by Ezquerro (2017); extensional and compressional stress tensors are distinguished. The following information is given for each data site: label used in the present work, in particular in Fig. 4; name according to Ezquerro (2017); UTM coordinates, affected rocks, age, lithostratigraphic and genetic unit, azimuth of the horizontal σ_3 or σ_1 axis, stress ratio, chronological order, and analytical method, as in Table 1; n/N: number of data explained by the stress tensor with respect to the total sample size.

Site			Location		Lithology	Age	Unit		Stress state			Angular misfit	n/N	Analysis method
Ref.	Nº	Original name	Coord. X	Coord. Y			1	2	Azimut	R_e	R			
Extensional stress tensors (σ_1 vertical)									**σ_3**					
1	P1	A01	661867	4470590	Lm	Turolian	P1	TN3	056	0.32	3.13	5º	11/15	ET
	P2	A02	661888	4470548	Lm	Turolian	P1	TN3	170	0.18	5.56	8º	7/9	ET
	P3	A03	661903	4470523	Lm	Turolian	P1	TN3	008	0	→∞	4º	12/16	ET
	P4	A04	661928	4470419	Lm	Turolian	P1	TN3	093	0.05	20.0	7º	9/11	ET
	P5	A05	661984	4470426	Lm	Turolian	P1	TN3	062	0.35	2.86	-	18/18	ET
	P6	A06	661201	4470221	Lm + Gy	Vallesian	CI	TN2	172 (1)	0	→∞	10º	21/47	ET
					Lm				064 (2)	0.02	50.0	10º	13/47	ET
	P7	A07	662042	4470368	Lm	Turolian	P1	TN3	099	0.03	33.3	9º	20/24	ET
	P8	A08	662211	4470339	Lm	Turolian	P1	TN3	036	0.03	33.3	6º	20/25	ET
	P9	A09	661621	4470022	Lm	Ruscinian	P2	TN4	122	0.09	11.1	5º	20/22	ET
	P10	A10	661663	4469924	Lm	Ruscinian	P2	TN4	098	0.08	12.5	7º	22/27	ET
	P11	A11	661447	4469112	Lm	Ruscinian	P2	TN4	110	0.07	14.2	2º	10/21	ET
	P12	A12	661882	4468510	Lm + Gy	Turolian	P1	TN3	133	0.01	100	10º	9/13	ET
	P13	A13	661312	4468977	Lm + Gy	Ruscinian	P2	TN4	138	0.16	6.25	14º	15/22	ET
	P14	A14	662438	4468363	Lm	Turolian	P1	TN3	126	0.05	20.0	8º	19/28	ET
	P15	A15	661078	4468654	Lm	Ruscinian	P2	TN4	034	0.03	33.3	7º	25/26	ET
	P16	A16	663053	4468219	Lm + Gy	Ruscinian	P2	TN4	049	0.03	33.3	8º	24/32	ET
	P17	T01	661519	4466583	Lm	Vallesian	UDI	TN2	094	0.10	10.0	-	8/8	ET
2	P18	04	653231	4472974	Co	Villafranchian	VG	TN5	000				39/39	LI
	P19	06	657728	4473332	Co + St	Villafranchian	VG	TN5	126 (1)				14/22	LI
									036 (2)				8/22	LI
	P20	07	657718	4472645	Co + Mu	Villafranchian	VG	TN5	022				50/50	LI
	P21	08	661805	4471587	Lm	Turolian	P1	TN3	146				12/12	LI
	P22	10	661452	4471286	Lm	Turolian	P1	TN3	075				8/8	LI
	P23	11	661452	4471286	Lm	Turolian	P1	TN3	071				11/11	LI
	P24	12	661452	4471286	Lm	Turolian	P1	TN3	015				13/13	LI
	P25	13	661452	4471286	Lm	Turolian	P1	TN3	175				11/11	LI
	P26	14	661452	4471286	Lm	Turolian	P1	TN3	090				16/16	LI
	P27	15	660822	4470257	Co	Villafranchian	R3	TN5	042				13/13	LI
	P28	16	659316	4472974	Lm	Turolian	P1	TN3	035				22/22	LI
	P29	17	661328	4472049	Lm	Turolian	P1	TN3	065				33/33	LI
	P30	18	659945	4470729	Mu	Villafranchian	R3	TN5	166				20/20	LI
3,6	P31	Orrios	668712	4494100	Lm	Ruscinian	P2	TN4	056 (1)	0.40	2.50	7º	12/58	ET
									112 (2)	0.20	5.00		9/58	yR
4	P32	12 Perales	670230	4502076	Co	Villafranchian	VG	TN5	067				10/10	LI
	P33	13 Villalba Alta 1	671947	4497718	Lm	Villafranchian	R3	TN5	004				24/24	LI
	P34	15 Escorihuela	672958	4487361	Co	Villafranchian	VG	TN5	075				14/14	LI
	P35	19 Valdecebro	671899	4469660	Co	Villafranchian	VG	TN5	072				12/12	LI
5	P36	Pobo 3	674717	4495591	Lm	Early Jurassic	CL		027	0.03	33.3	12º	7/9	ET
	P37	Pobo 5	676968	4493436	Lm	Early Jurassic	CL		120	0.50	2.00		2/17	yR
	P38	Pobo 7	675738	4487342	Lm	Early Jurassic	CL		124 (1)	0.45	2.22	12º	15/51	ET
									010 (2)	0.22	4.50	3º	6/51	ET
	P39	Pobo 8	677388	4487342	Lm	Early Jurassic	CL		096	0.40	2.50		7/37	yR
	P40	Pobo 9	676787	4485387	Lm	Early Jurassic	CL		107	0.24	4.17	11º	18/42	ET
6	P41	567/06	663200	4469600	Lm	Turolian	P1	TN3	102	0.14	7.14	6º	8/11	ET
	P42	567/07	658400	4478200	Lm + Mu	Villafranchian			040				10/10	LI
4		08 Caudé			Co	Villafranchian	VG	TN5	000				25	LI
		09 Bco. del Monte			Co + St	Mid. Pleistoc.	T		073				32	LI
		11 Concud 2			Co + Mu	Villafranchian	VG	TN5	022				38	LI
		14 Orrios			Co + St	Mid. Pleistoc.	T		175				35	LI
		16 Los Baños 1			Co	Mid. Pleistoc.	T		145				10	LI
		17 Los Baños 2			Co	Mid. Pleistoc.	T		053				10	LI
		18 Teruel			Co + St	Mid. Pleistoc.	T		066				13	LI
2		01			Mu + Co	Villafranchian	VG	TN5	073				28	LI
		02			Mu + Co	Villafranchian	VG	TN5	065				26	LI
		03			Co	Villafranchian	VG	TN5	066				26	LI
		05			Co + Mu	Mid. Pleistoc.	T		073				35	LI
		09			Co	Mid. Pleistoc.	T		057				12	LI
		19			Co + Mu	Mid. Pleistoc.	T		066				23	LI
Compressional and strike-slip stress tensors (σ_1 horizontal)									**σ_1**					
6,7	P31	Orrios	668712	4494100	Lm	Ruscinian	P2	TN4	033 (1)	0.96	0.96	9º	11/58	ET
									001 (2)	0.52	0.52	8º	8/58	ET

TABLE 1

Site		Location		Lithology	Age	Unit		Stress state			Angular misfit (º)	nº/ N	Analysis method
Nº	Name	Coord. X	Coord. Y			1	2	Azimut	R_e	R			
Extensional stress tensors (σ_1 vertical)								**σ_3**					
1	Alcamines río	673795	4500189	Mu + St	Vallesian	UDI	?	086	0.58	1.72	6º	11/17	ET
2	Villalba Alta macroestación	673265	4498417	Mu + Co	Late Ruscinian	UDI	TN5	087	0	→∞		20/36	LI
3	Villalba Alta granja	672271	4498208	Lm	Late Ruscinian	P2	TN4	125 (1)	0	→∞	8º	25/35	ET
								089 (2)	0	→∞	10º	26/35	ET
5	Corral del Majano	662718	4490981	Co	Vallesian	UDI	TN1	135	0	→∞		16/21	LI
6	Corrales de Cabigordo	663273	4487905	Mu + Co	Vallesian	UDI	TN1	062	0	→∞		7/14	LI
7	Bco. Hondo	671492	4484088	Co	Early Turolian	UDI	TN4	124	0.05	20.00		12/12	LI
8	Muela umbría norte	665827	4488356	Lm	Turolian	P1	TN3	121	0.07	14.29	12º	15/21	ET
9	Peralejos merendero	666871	4483058	Lm	Vallesian	KI	TN2	176 (1)	0.07	14.29	8º	10/28	ET
								095 (2)	0.07	14.29		26/28	ET
10	Venta Alta	666070	4483597	Lm	Early Ruscinian	P2	TN4	040	0	→∞	8º	14/17	ET
11	Cueva Tinajo	668321	4483983	Lm	Turolian	P1	TN3	016	0.03	33.33	10º	22/27	ET
12	Cañamaria	656953	4480493	Lm	Early Ruscinian	P2	TN4	111	0.05	20.00	7º	25/27	ET
13	Sta. Quiteria afluente	663772	4479859	Lm	Early Ruscinian	P2	TN4	085	0.15	6.67	10º	16/18	ET
14	Sta. Quiteria calizas	663762	4479949	Lm	Late Turolian	R2	TN4	136 (1)	0.04	25.00	6º	15/25	ET
								085 (2)	0.05	20.00	8º	14/25	ET
15	Sta. Quiteria margas	663762	4479949	Lm	Late Turolian	R2	TN4	178 (1)	0	→∞		17/20	LI
								034 (2)	0.12	8.33	6º	7/9	ET
16	Bco. de los Chopos	663643	4478853	Mu + Lm	Late Turolian	R2	TN4	090	0.04	25.00		9/15	LI
17	Villalba Baja delta IV	663390	4477501	Mu + Lm	Late Turolian	R2	TN4	058	0	→∞		8/14	LI
18	Villalba Baja delta III	663385	4477496	Mu + Lm	Late Turolian	R2	TN4	038	0	→∞		16/21	LI
19	Villalba Baja delta II	663362	4477480	Mu + Lm	Late Turolian	R2	TN4	019				4/4	CF
20	Villalba Baja delta I	663334	4477442	Mu + Lm	Late Turolian	R2	TN4	025	0.05	20.00		21/29	LI
21	Villalba Baja rio	663195	4476871	Mu + Lm	Turolian	P1	TN2	046	0.02	50.00		27/34	LI
22	Mas de la Casa Baja	672446	4471615	Co	Vallesian	UDI	?	121	0	→∞		8/17	LI
23	Valdecebro Talud	664431	4469654	Mu	Vallesian	UDI	TN1	087 (2)	0.33	3.03	5º	6/23	ET
								058 (3)	0.03	33.33		24/41	LI
24	Cuevas de las Tres Puertas	661796	4468275	Lm + Gy	Turolian	P1	TN3	058	0.17	5.88	11º	17/23	ET
Compressional and strike-slip stress tensors (σ_1 horizontal)								**σ_1**					
4	Castillo de Alfambra	666125	4490261	Mu	Vallesian	UDI	TN3	027	0.74	-2.85		6/11	LI
23	Valdecebro Talud	664431	4469654	Mu		UDI	TN1	166 (1)	0.86	0.86	8º	12/23	ET

TABLE 2

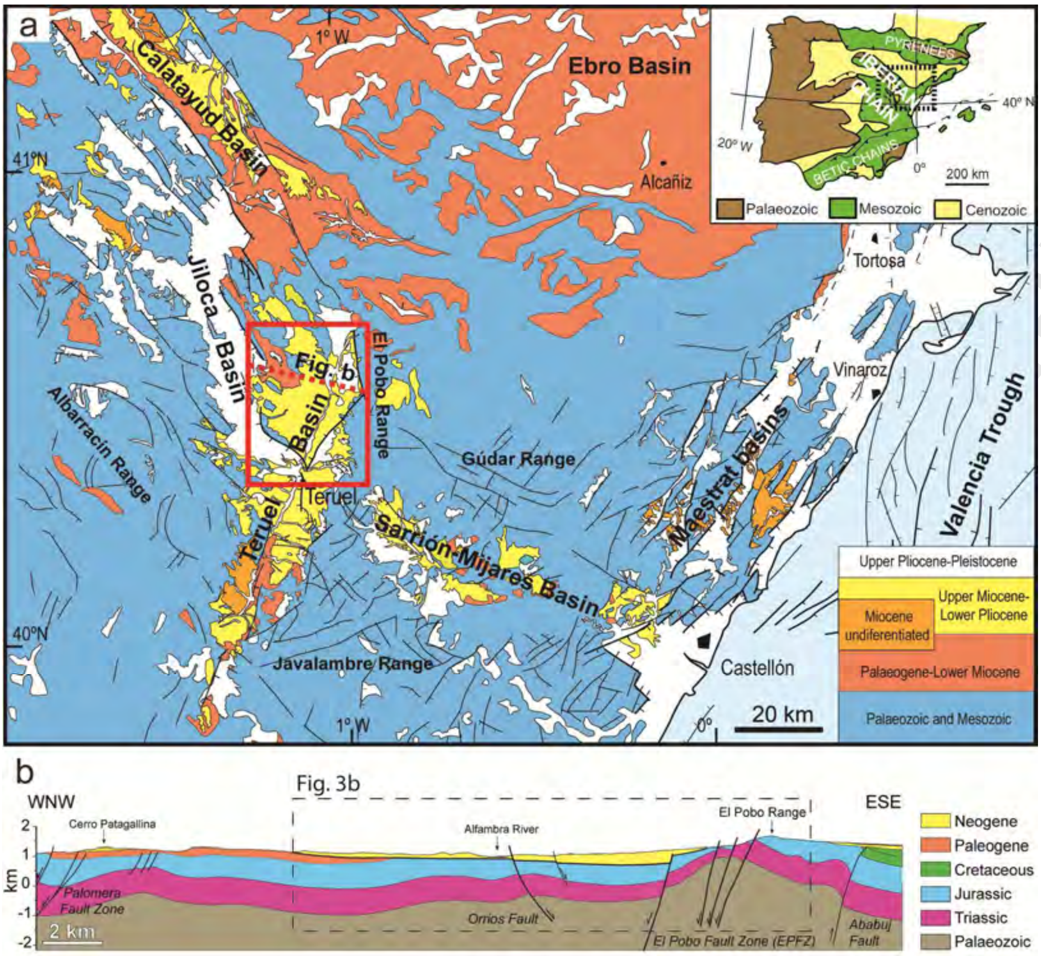
a
1º W
Ebro Basin
Calatayud Basin
41ºN
Alcañiz
Jiloca Basin
Fig. b
Basin
El Pobo Range
Albarracín Range
Gúdar Range
Teruel
Teruel
Sarrión-Mijares Basin
Maestrat basins
Tortosa
Vinaroz
Valencia Trough
40ºN
Javalambre Range
Castellón
1º W
0º
20 km
PYRENEES
IBERIAN CHAIN
BETIC CHAINS
40º N
20º W
0º
200 km
Palaeozoic
Mesozoic
Cenozoic
Upper Pliocene-Pleistocene
Upper Miocene-Lower Pliocene
Miocene undiferentiated
Palaeogene-Lower Miocene
Palaeozoic and Mesozoic
b
Fig. 3b
WNW
ESE
Cerro Patagallina
Alfambra River
El Pobo Range
km
2
1
0
-1
-2
Palomera Fault Zone
2 km
Orrios Fault
El Pobo Fault Zone (EPFZ)
Ababuj Fault
Neogene
Paleogene
Cretaceous
Jurassic
Triassic
Palaeozoic

Figure 1

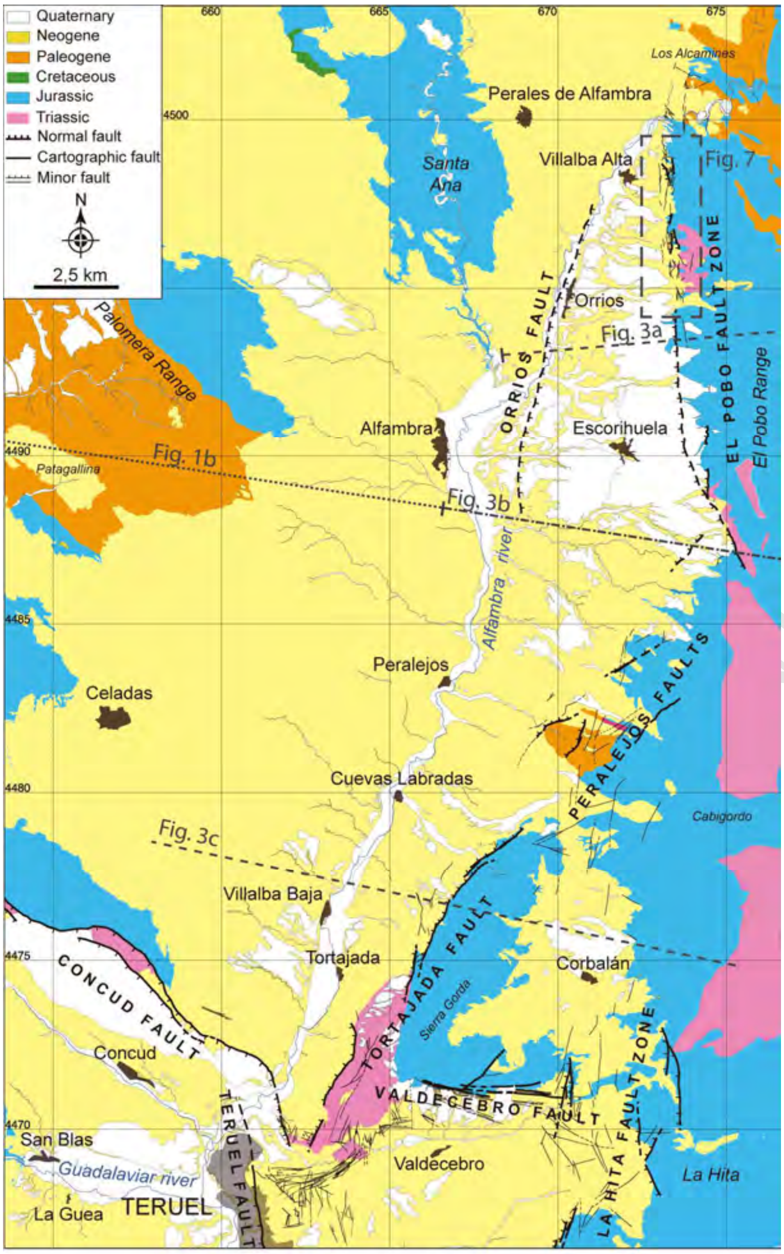

Quaternary
Neogene
Paleogene
Cretaceous
Jurassic
Triassic
Normal fault
Cartographic fault
Minor fault
N
2,5 km
660
665
670
675
4500
4490
4485
4480
4475
4470
Los Alcamines
Perales de Alfambra
Villalba Alta
Fig. 7
Santa Ana
Orrios
ORRIOS FAULT
Fig. 3a
EL POBO FAULT ZONE
El Pobo Range
Palomera Range
Alfambra
Escorihuela
Fig. 1b
Patagallina
Fig. 3b
Alfambra river
Peralejos
Celadas
PERALEJOS FAULTS
Cuevas Labradas
Cabigordo
Fig. 3c
Villalba Baja
Tortajada
TORTAJADA FAULT
Corbalán
CONCUD FAULT
Sierra Gorda
Concud
VALDECEBRO FAULT
LA HITA FAULT ZONE
TERUEL FAULT
San Blas
Guadalaviar river
Valdecebro
La Hita
La Guea
TERUEL

Figure 2

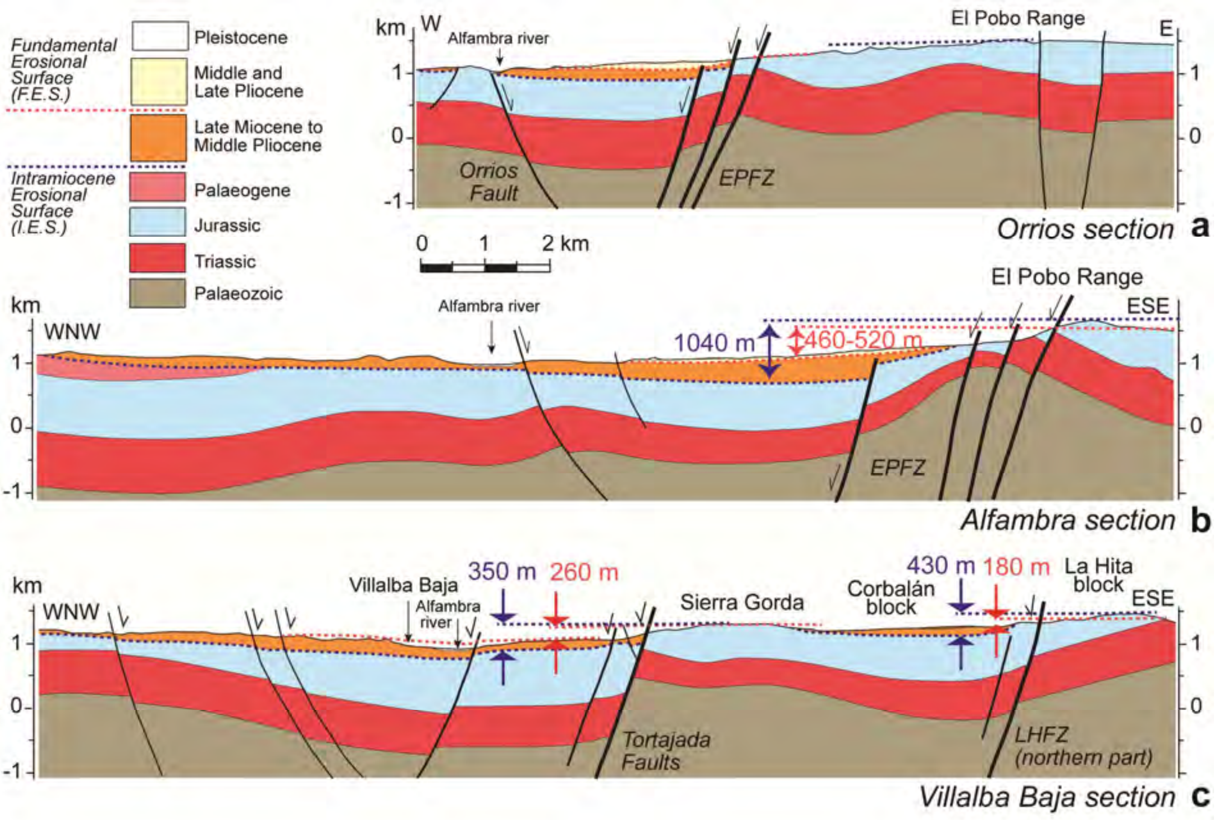
Fundamental Erosional Surface (F.E.S.)
Intramiocene Erosional Surface (I.E.S.)
Pleistocene
Middle and Late Pliocene
Late Miocene to Middle Pliocene
Palaeogene
Jurassic
Triassic
Palaeozoic
km
W
E
Alfambra river
El Pobo Range
Orrios Fault
EPFZ
0 1 2 km
Orrios section a
WNW
ESE
1040 m
460-520 m
Alfambra section b
Villalba Baja
350 m
260 m
Sierra Gorda
Corbalán block
430 m
180 m
La Hita block
Tortajada Faults
LHFZ (northern part)
Villalba Baja section c

Figure 3

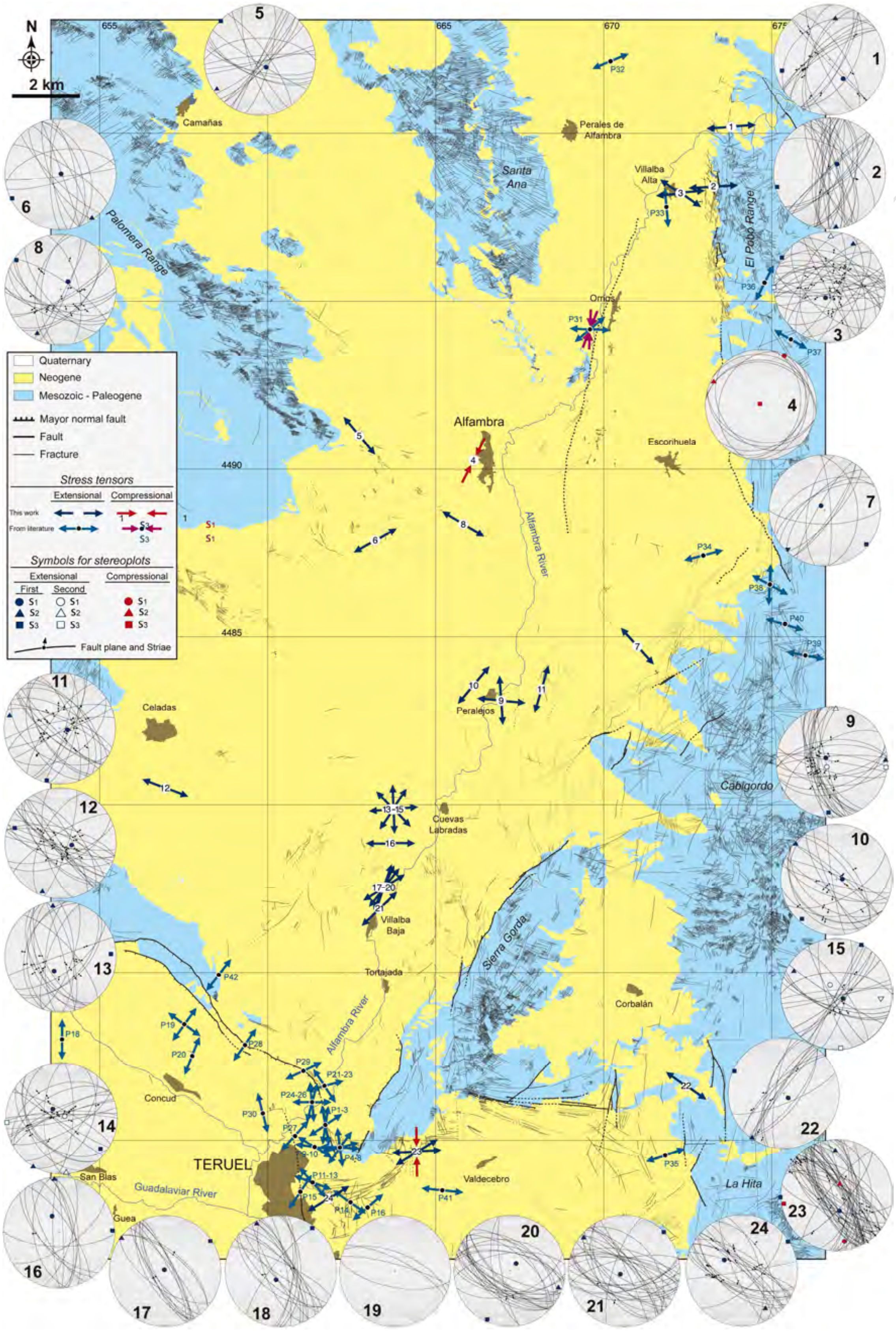

N
2 km
655
665
670
675
Camañas
Perales de Alfambra
Santa Ana
Villalba Alta
El Pobo Range
Palomera Range
Orrios
Quaternary
Neogene
Mesozoic - Paleogene
Mayor normal fault
Fault
Fracture
Stress tensors
Extensional
Compressional
This work
From literature
Symbols for stereoplots
Extensional
Compressional
First
Second
Fault plane and Striae
Alfambra
Escorihuela
4490
4485
Alfambra River
Peralejos
Celadas
Cabigordo
Cuevas Labradas
Villalba Baja
Tortajada
Sierra Gorda
Corbalán
Concud
TERUEL
San Blas
Guadalaviar River
Guea
Valdecebro
La Hita

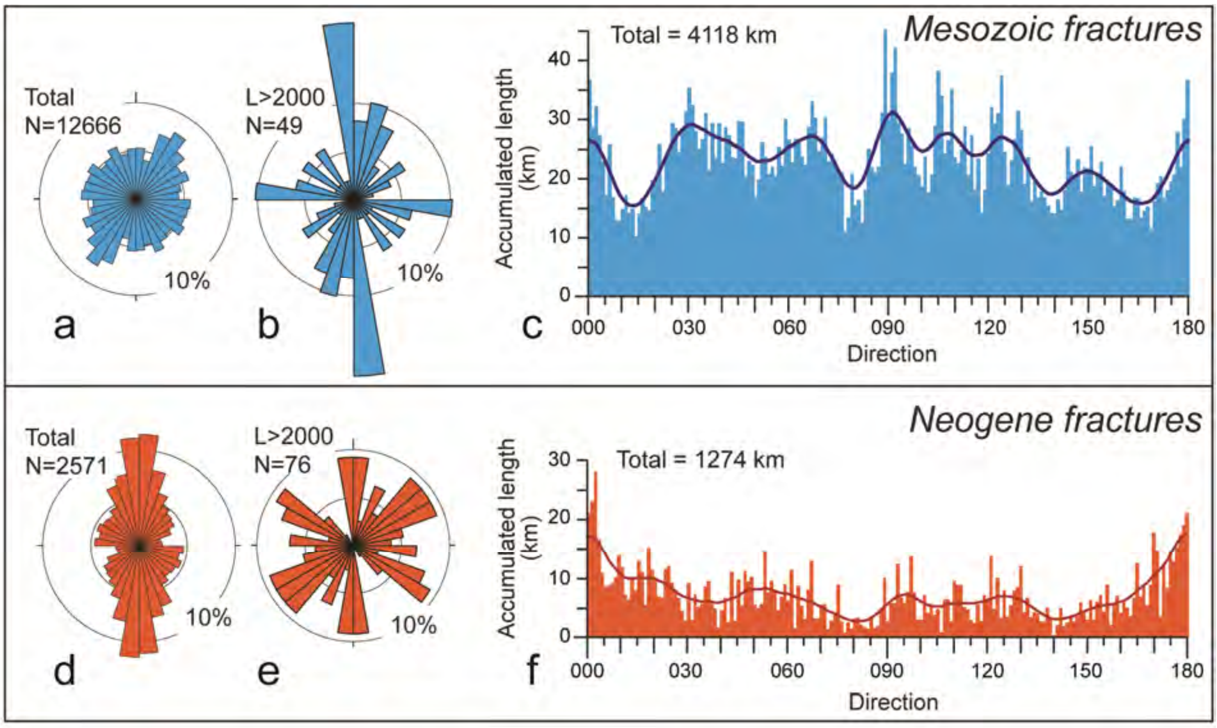
Total
N=12666
10%
a
L>2000
N=49
10%
b
Total = 4118 km
Mesozoic fractures
Accumulated length (km)
40
30
20
10
0
c
000
030
060
090
120
150
180
Direction
Total
N=2571
10%
d
L>2000
N=76
10%
e
Neogene fractures
Total = 1274 km
Accumulated length (km)
30
20
10
0
f
000
030
060
090
120
150
180
Direction

Figure 5

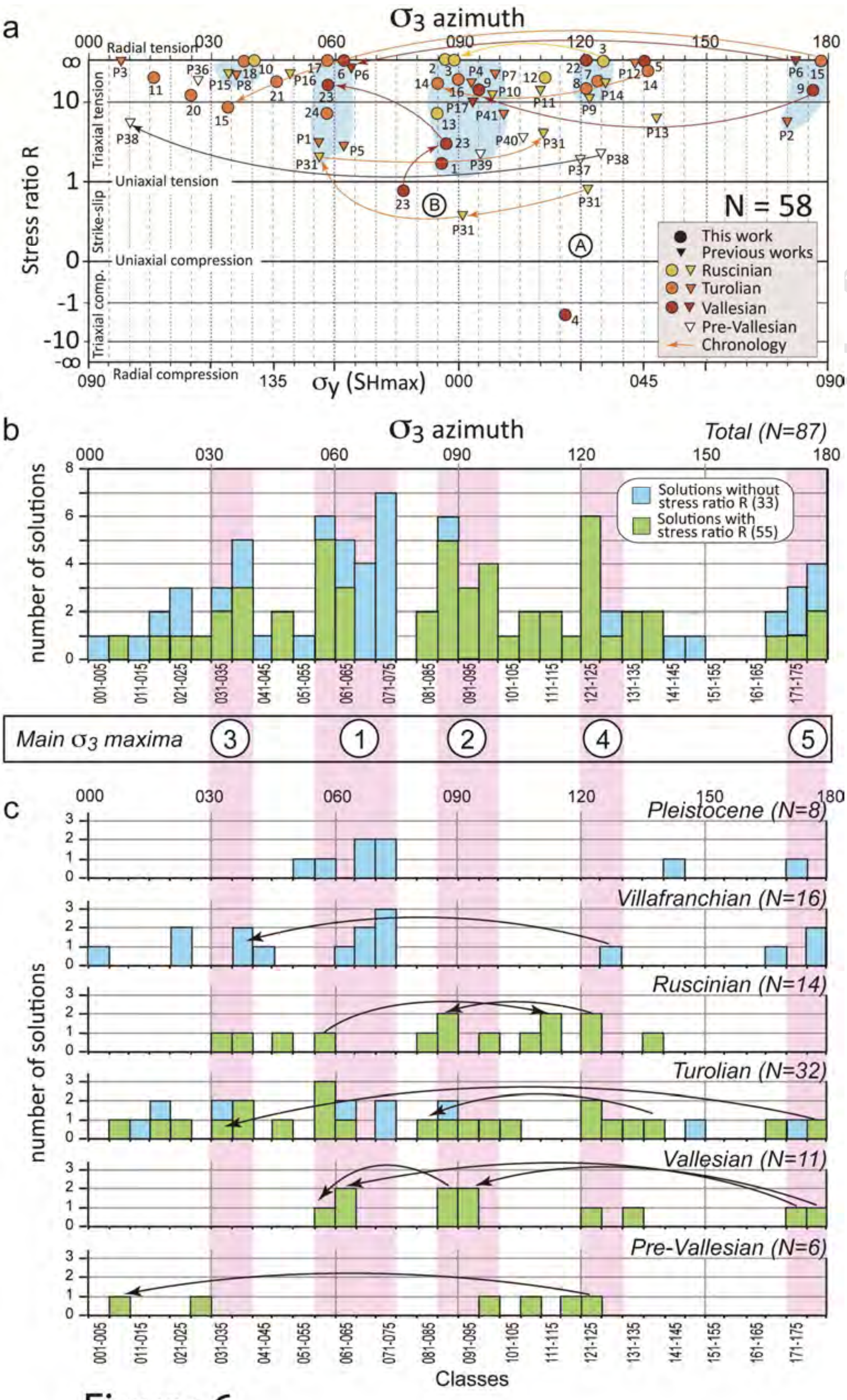

a
σ3 azimuth
Stress ratio R
Radial tension
Triaxial tension
Uniaxial tension
Strike-slip
Uniaxial compression
Triaxial comp.
Radial compression
σy (SHmax)
N = 58
This work
Previous works
Ruscinian
Turolian
Vallesian
Pre-Vallesian
Chronology
b
σ3 azimuth
Total (N=87)
number of solutions
Solutions without stress ratio R (33)
Solutions with stress ratio R (55)
Main σ3 maxima
c
Pleistocene (N=8)
Villafranchian (N=16)
Ruscinian (N=14)
Turolian (N=32)
Vallesian (N=11)
Pre-Vallesian (N=6)
number of solutions
Classes

Figure 6

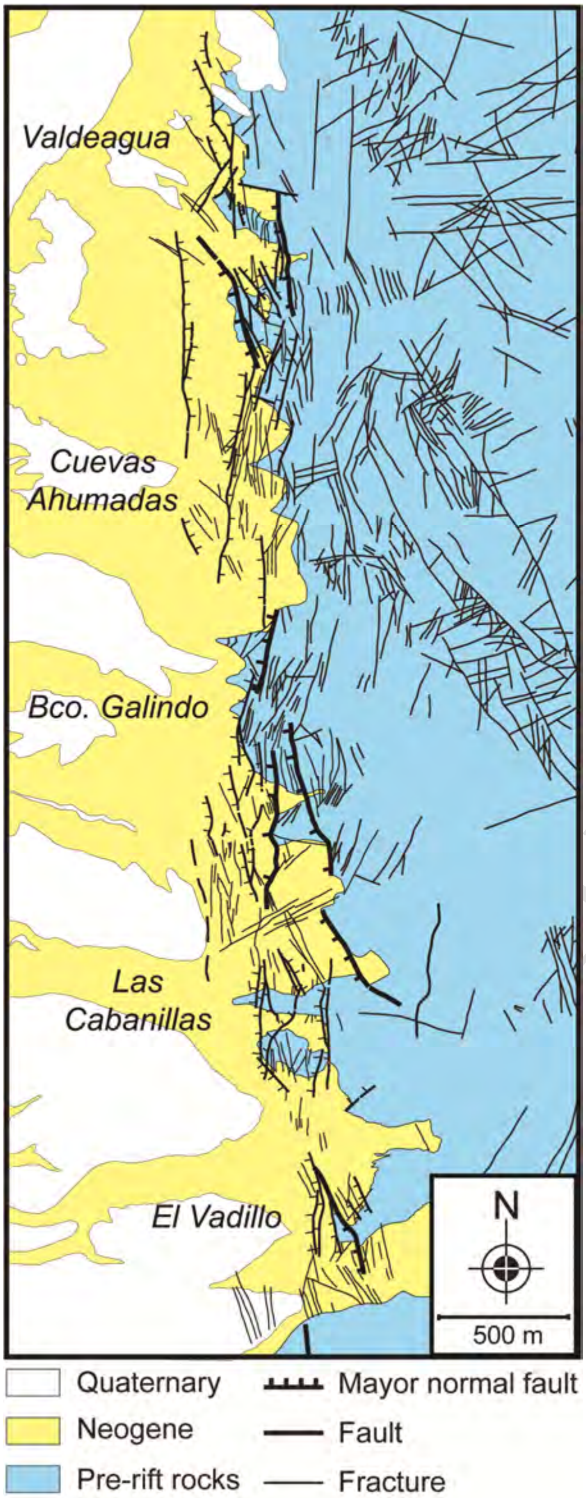
Valdeagua
Cuevas
Ahumadas
Bco. Galindo
Las
Cabanillas
El Vadillo
N
500 m
Quaternary
Neogene
Pre-rift rocks
Mayor normal fault
Fault
Fracture

Figure 7

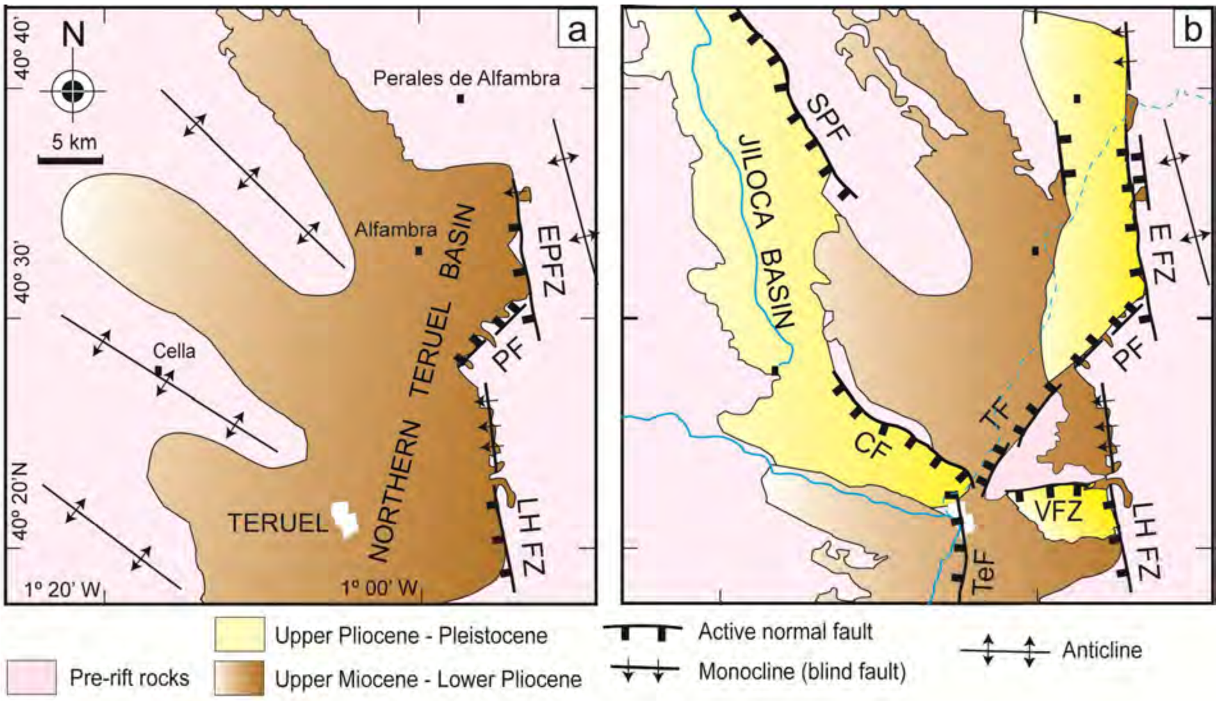
a
N
5 km
40° 40'
40° 30'
40° 20'N
1° 20' W
1° 00' W
Perales de Alfambra
Alfambra
Cella
TERUEL
NORTHERN TERUEL BASIN
EPFZ
PF
LH FZ
b
SPF
JILOCA BASIN
E FZ
PF
TF
CF
VFZ
LH FZ
TeF
Pre-rift rocks
Upper Pliocene - Pleistocene
Upper Miocene - Lower Pliocene
Active normal fault
Monocline (blind fault)
Anticline

Figure 8

Highlights

Diverse orientation, border and intrabasinal faults in the Neogene Teruel basin.

Use of stratigraphical–geomorphological markers for analysing fault activity.

Characterization of Neogene deformation and structural inheritance from fracturing.

Structural inheritance and evolving stress systems as controls on basin evolution.